

**CHRONIC NOISE STRESS AFFECTS NEOCORTICAL AND HIPPOCAMPAL-  
AMYGDALA FUNCTIONAL CONNECTIVITY IN MICE**

**MEGAN SHOLOMISKI**  
**Bachelor of Science, University of Lethbridge, 2018**

A thesis submitted  
in partial fulfillment of the requirements for the degree of

**MASTER OF SCIENCE**

in

**NEUROSCIENCE**

Department of Neuroscience  
University of Lethbridge  
LETHBRIDGE, ALBERTA, CANADA

© Megan Sholomiski, 2020

CHRONIC NOISE STRESS AFFECTS BEHAVIOUR AND HIPPOCAMPAL-  
CORTICAL-AMYGDALA FUNCTIONAL CONNECTIVITY IN MICE

MEGAN SHOLOMISKI

Date of Defence: December 17, 2020

Dr. B. Kolb	Professor	Ph.D.
Dr. M. Mohajerani	Associate Professor	Ph.D.
Thesis Co-Supervisors		

Dr. I. Wishaw	Professor	Ph.D.
Thesis Examination Committee Member		

Dr. R. Sutherland	Professor	Ph.D.
Thesis Examination Committee Member		

Dr. David Euston	Associate Professor	Ph.D.
Chair, Thesis Examination Committee		

## **Dedication**

To my grandpa, John Sholomiski, who not only melts me with his supportive weekly phone calls, but also might be the only person more excited about this thesis than me.

## **Abstract**

This thesis examines the effects of chronic noise stress on neocortical and hippocampal-amygdala networks and their behavioural correlates. Psychological symptoms of stress, including anxiety and depression, are thought to be caused by alterations in functional connectivity within the brain. A functional pathway has been established between the basolateral amygdala, which mediates emotional responses to stressors, the ventral hippocampus which provides context to emotional memories and experiences, and medial prefrontal cortex, which alters attention and perception of stressors. This network is adaptive in the presence of an acute stressor, allowing an organism to optimally prepare and deal with the source of stress, but may become dysfunctional when exposed to chronic stress. The hypotheses that chronic noise stress correlates to neocortical hyperconnectivity and decreased synchrony between the amygdala and hippocampus, correlates to altered behaviour, and correlates to altered brain morphology were tested in head-fixed mice using optical imaging and behavioural recordings.

## **Acknowledgements**

I would like to thank my supervisor, Dr. Majid Mohajerani, my co-supervisor, Dr. Bryan Kolb, and my supervisory committee members, Dr. Ian Wishaw and Dr. Robert Sutherland for their support and guidance throughout my graduate program. Thank you to Ali Mashhoori, for his love, support, and assistance with all MATLAB-related analysis. I would also like to my friends and colleagues within the Mohajerani lab and throughout the CCBN for their kindness, advice, collaboration, and for waffle Sundays.

## Table of Contents

Dedication .....	iii
Abstract .....	iv
Acknowledgements .....	v
Table of Contents .....	vi
List of Tables .....	viii
List of Figures .....	ix
List of Abbreviations .....	xi
1. Introduction .....	1
1.1. Stress .....	1
1.1.1. Noise as a stressor .....	5
1.1.2. Modeling stress in mice .....	8
1.2. The hippocampal-cortical-amygdala network .....	9
1.2.1. The ventral hippocampus .....	10
1.2.2. The neocortex .....	12
1.2.3. The basolateral amygdala .....	15
1.3. Theory .....	17
1.4 Rationale .....	18
1.5. Hypotheses .....	18
2. Chronic noise stress experiment .....	20
2.1. Introduction to experiment .....	20
2.2. Glutamate imaging .....	21
2.3. Methods .....	22
2.3.1. Animals .....	22
2.3.2. Chronic noise stress group .....	22
2.3.3. Control group .....	23
2.3.4. Electrode fabrication .....	23
2.3.5. Surgical procedure .....	24
2.3.6. Recordings .....	25
2.3.6.1. <i>Sensory evoked mapping</i> .....	26
2.3.6.2. <i>Widefield imaging analysis</i> .....	28
2.3.6.3 <i>Electrophysiology analysis</i> .....	29

2.3.6.5. <i>Behavioural analysis</i> .....	30
2.3.7. <i>Histology and morphological analysis</i> .....	31
2.4. Results .....	35
2.4.1. Pupil activity .....	35
2.4.2. Brain morphology .....	38
2.4.3. Cortical connectivity.....	45
2.4.4. Electrophysiology .....	52
3. Discussion .....	56
3.1. Chronic and acute noise exposure alters pupil activity .....	57
3.2. Chronic noise stress creates changes in brain morphology .....	59
3.3. Chronic noise exposure correlates to changes in cortical network connectivity.....	63
3.4. Chronic and acute noise exposure alters HPC-BLA connectivity .....	64
4. Conclusion .....	68
5. References.....	69

## **List of Tables**

Table 1. Statistical values for CNS animals between spontaneous recordings.....	45
Table 2. Statistical values for CNS animals between noise recordings.....	45

## List of Figures

Figure 1. The hypothalamic-pituitary-adrenal axis.....	4
Figure 2. Auditory system connections to stress systems in the brain.....	7
Figure 3. The mouse hippocampus.....	11
Figure 4. The mouse neocortex.....	13
Figure 5. The mouse amygdala.....	16
Figure 6. Overview of chronic noise experiments.....	20
Figure 7. Schematic of chronic surgical implants.....	25
Figure 8. Chronic head-fixed recording schematic.....	26
Figure 9. Sensory evoked map of the mouse neocortex.....	28
Figure 10. Example montage of spontaneous cortical activity.....	29
Figure 11. Example LFP theta signals and leading/lagging analysis.....	30
Figure 12. Histology for electrodes and imaging.....	32
Figure 13. Rough morphological analysis.....	34
Figure 14. Pupil activity for control animals during recordings.....	36
Figure 15. Pupil activity for CNS animals during recordings.....	37
Figure 16. Mean brain volumes of stress and control animals.....	38
Figure 17. Mean amygdala volumes of stress and controls.....	39
Figure 18. Mean hippocampal volumes of stress and controls.....	40
Figure 19. Cortical thickness measures 2.46 mm from bregma.....	41
Figure 20. Cortical thickness measures 2.22 mm from bregma.....	41
Figure 21. Cortical thickness measures 1.42 mm from bregma.....	42
Figure 22. Cortical thickness measures 1.10 mm from bregma.....	42
Figure 23. Cortical thickness measures 0.50 mm from bregma.....	43
Figure 24. Cortical thickness measures -0.10 mm from bregma.....	43
Figure 25. Cortical thickness measures -0.70 mm from bregma.....	44
Figure 26. Cortical correlations for control animals.....	46
Figure 27. Average cortical correlation for control animals.....	47
Figure 28. Cortical correlations for stress animals.....	49

Figure 29. Average cortical correlation for stress animals..... 51  
Figure 30. Leading/lagging theta activity in BLA and vHPC of control animals.... 53  
Figure 31. Leading/lagging theta activity in BLA and vHPC of CNS animals..... 55

## List of Abbreviations

ACTH	Adrenocorticotrophic hormone
aM2/AC	Secondary motor/anterior cingulate
AMPAR	$\alpha$ -amino-3-hydroxy-5-methyl-4-isoxazolepropionic acid receptor
AP	Anterior/posterior
AVP	Arginine vasopressin
BC C2 S2	Secondary barrel sensory
BDNF	Brain-derived neurotrophic factor
BLA	Basolateral amygdala
CNS	Chronic noise stress
CORT	Cortisol or corticosterone
CRH	Corticotropin-releasing hormone
DMN	Default mode network
EEG	Electroencephalogram
FL S2A	Secondary forelimb sensory
GAS	General Adaptation Syndrome
Glu	Glutamate
GR	Glucocorticoid receptor
HPA-axis	Hypothalamic-pituitary-adrenal axis
IP	Intraperitoneal
LFP	Local field potential
mBC	Barrel motor
MDD	Major depressive disorder
mFL	Forelimb motor
mHL	Hindlimb motor
mPFC	Medial prefrontal cortex
MR	Mineralocorticoid receptor
MRI	Magnetic resonance imaging
NMDAR	N-methyl-D-aspartate receptor

PBS	Phosphate-buffered saline
PFA	Paraformaldehyde
PM2	Posterior secondary motor
ptA	Parietal association area
PTSD	Post-traumatic stress disorder
PVN	Paraventricular nucleus of the hypothalamus
RC	Rostral/caudal
ROI	Region of interest
RS	Retrosplenium
S1J S1	Primary shoulder/neck sensory
SPL	Sound pressure level
SWR	Sharp-wave ripple
TN	Traffic noise
V2L	Lateral secondary visual
V2MM & V2LM	Medial secondary visual
vHPC	Ventral hippocampus
VSDI	Voltage-sensitive dye imaging

# 1. Introduction

Chronic environmental noise exposure is a pervasive and growing threat to public health. Unwanted sound is linked to cardiovascular disease, diabetes, increased blood pressure, stress, nausea, exhaustion, attentional deficits, and mood disorders (Stallen 1999, Goines and Hagler 2007, Naqvi, Haider et al. 2012). Psychological symptoms of stress, including anxiety, depression, and post-traumatic stress disorder (PTSD) are thought to be caused by alterations in functional connectivity within the brain (Kaiser, Andrews-Hanna et al. 2015, Takagi, Sakai et al. 2018). More than one million healthy life years are lost per year to traffic noise stress in European-A member states, an exemplar population (Grandjean, Azzinnari et al. 2016), so understanding the impact of noise stress on the brain is important to improve quality of life and reduce medical costs. Identifying the neural system-level coordinates of chronic stress is critical for understanding the implications of noise stress and promoting public health (Basner, Brink et al. 2015, Godoy, Rossignoli et al. 2018).

## 1.1. Stress

The term *stress* was first coined in a biologically relevant manner by Hans Selye when describing the nonspecific effects of physically or psychologically demanding stimuli on the nervous system (Selye 1950). He argued that these noxious stimuli have common effects on the nervous system, eliciting a hormonal stress response that occurs in three stages: (1) the alarm stage, which characterizes the acute fight-or-flight effect, (2) the resistance stage, in which the body attempts to adapt to the noxious stimulus and return to homeostasis, and (3) the exhaustion stage, when the organism has depleted the biological

resources necessary to maintain the stress response. This General Adaptation Syndrome (GAS) is beneficial in addressing acute stressors by enhancing the organism's performance and resilience in the short-term, while allowing it time to return to its pre-stress homeostasis when the noxious stimulus subsides. However, the GAS may be maladaptive in the cases of chronic stress, where organisms experience prolonged exposure to the biochemical mediators of the stress response.

One mediator of the stress response is the sympathetic adreno-medullar (SAM) system, which prepares an organism for the fight-or-flight reaction to a stressor in the alarm stage of the GAS. Beginning with the perception of a stressor, the amygdala communicates with the hypothalamus to transmit signals through nerve pathways in the spinal cord to reach target postsynaptic neurons in sympathetic nerve bundles. These nerve bundles then release the neurotransmitter acetylcholine into synapses formed with adrenal medulla, signalling the production and release of epinephrine and norepinephrine into systemic circulation. These amine hormones act on adrenergic receptors, which prepare the body for a physical response to a stressor.

A concurrent but slower acting mediator of the hormonal stress response is the hypothalamic-pituitary-adrenal (HPA) axis (Figure 1). When the brain perceives stress, the paraventricular nucleus of the hypothalamus (PVN) releases corticotropin-releasing hormone (CRH) and arginine vasopressin (AVP) into the hypophysial portal blood to signal the anterior pituitary to release adrenocorticotrophic hormone (ACTH). ACTH travels through the bloodstream to the adrenal cortex, signaling glucocorticoid hormone release. The main glucocorticoid stress hormone released by the adrenal glands is cortisol in humans and corticosterone in rodents (CORT), which produces the prolonged

physiological stress response following the immediate fight-or-flight effects of the SAM system. CORT is lipophilic, so it can cross the blood brain barrier to impact the brain via glucocorticoid (GR) and mineralocorticoid receptors (MRs). GRs in the hippocampus (HPC), amygdala, cortex, and PVN are primarily involved in stress perception and behaviour, while MRs throughout the body regulate the physiological stress response (McEwen 2007, Herman, McKlveen et al. 2016). This elevated CORT has a lingering effect responsible in part for the sustained stress adaptation characteristic of the GAS resistance stage. Following an acute stress event, CORT primarily acts on GRs to elicit negative feedback through suppression of CRH and AVP in the PVN and ACTH in the anterior pituitary, allowing the organism to enter the exhaustion stage of the GAS before returning to homeostasis (Herman, McKlveen et al. 2016).

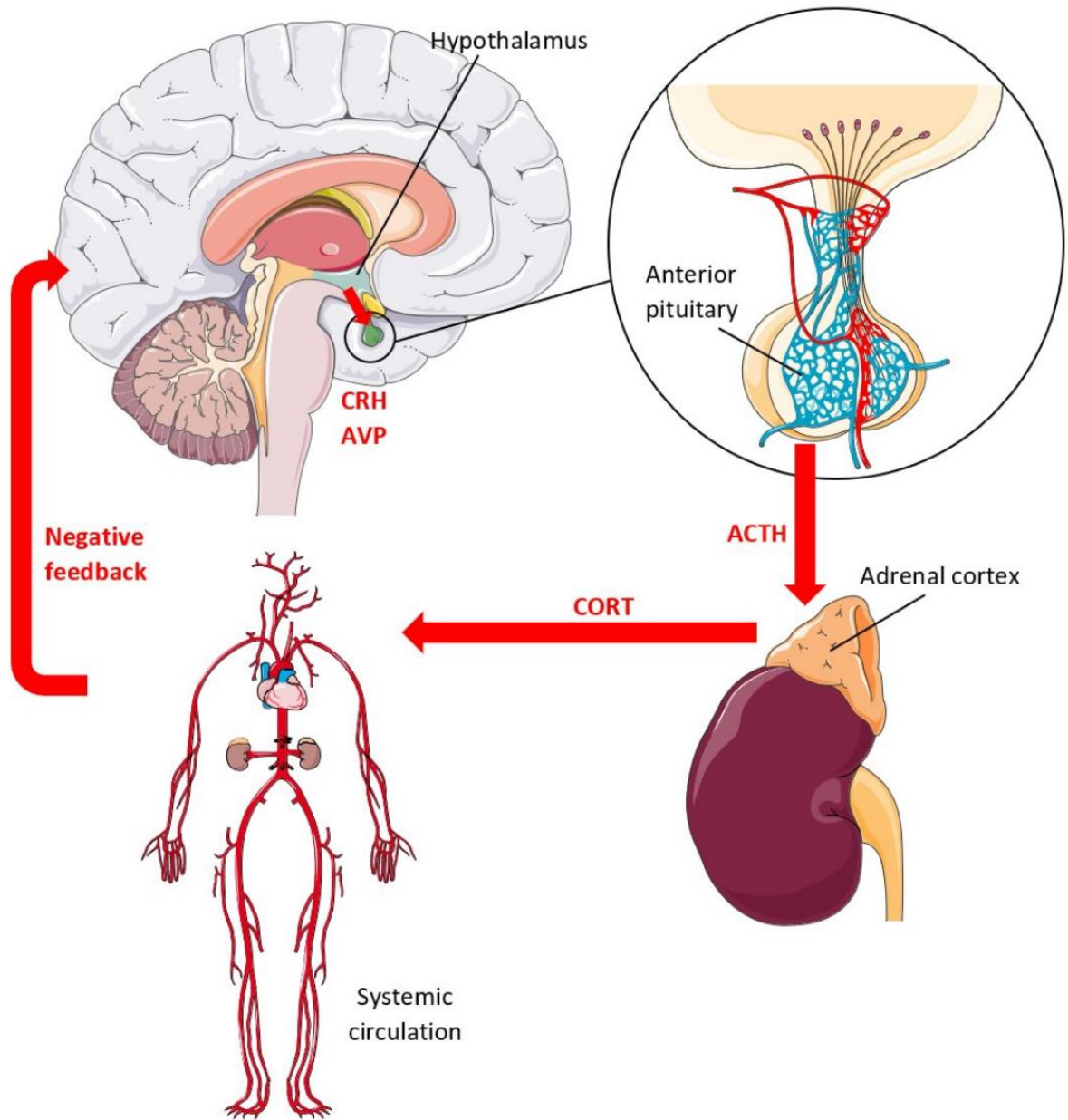


**Figure 1: The hypothalamic-pituitary-adrenal axis.** Stress perception in the brain activates the HPA-axis, which mediates the body’s sustained hormonal stress response. The hypothalamus secretes CRH and AVP, which signal the anterior pituitary to release ACTH. ACTH acts on receptors in the adrenal cortex, which releases CORT to elicit the physiological stress response and provide negative feedback to the brain. This figure was created using images from Servier Medical Art Commons.

The adaptative processes of the SAM system and HPA-axis to maintain homeostasis are referred to as *allostasis*, while the physiological and neurological effects of a stressor are referred to as its *allostatic load* (McEwen 2007). A chronic allostatic load can overload the HPA-axis with excess CORT, and over time result in a loss of GRs, thus damaging regulatory feedback and baseline functioning of the HPA-axis. This damage is characteristic of an *allostatic overload*, a condition that has been shown to result in mood disorders that correlate to alterations in the structure and connectivity of the cortex and limbic system (Young 2004, Patel, Kas et al. 2019). Resilience to allostatic load is dependent on factors including the duration and severity of a stressor and an individual's genetics, early life experience, environmental conditions, sex, and age (Herman, McKlveen et al. 2016).

### **1.1.1. Noise as a stressor**

Although any stimulus perceived as stressful will activate nonspecific stress systems, individual stressors also create effects specific to the insult. These specific effects are directly produced by the noxious stimulus, for example cochlear damage and a loss of hearing caused by exposure to loud noise. Ultimately, the brain's response to any stressor is a result of both its specific and nonspecific effects. Although physical and psychological stressors have common nonspecific effects on the nervous and endocrine systems, it has been shown that different stressors may have unique correlates of neural activity (Godoy, Rossignoli et al. 2018, Patel, Kas et al. 2019). Psychological stressors, which elicit the stress response without the threat of physical harm, tend to take longer to produce an identifiable stress response but also tend to have a more severe short- and long-term consequences in the brain (Lamb 1979, Li, Qin et al. 2019). Psychological

stressors are commonly used in models of anxiety and depression to test pharmaceutical treatments in rodents independent of the potential confounds of physical stressors (Nollet, Le Guisquet et al. 2013, Antoniuk, Bijata et al. 2019).

One evolutionary purpose for hearing is that it developed as a means of perceiving and responding to potential threats to survival, therefore the auditory system is adapted to processing unpredictable noise as stressful (Westman and Walters 1981). Noise, an auditory stimulus that overloads the brain's processing abilities, at a high enough level to elicit the nonspecific stress response while not high enough to cause hearing damage is an established paradigm for studying psychological stress (Dong, Zhou et al. 2016, Jafari, Kolb et al. 2017, Munzel, Daiber et al. 2017, Jafari, Kolb et al. 2018).

Chronic noise stress (CNS) has been shown to trigger psychological alterations and disorders including anger, disappointment, dissatisfaction, withdrawal, helplessness, depression, anxiety, distraction, agitation, and exhaustion (Goines and Hagler 2007, Seidler, Hegewald et al. 2017). The behavioural effects of CNS have been linked to alterations in brain stress networks and hyperactivity in the central auditory pathway (Malone, Heiser et al. 2017). The auditory system forms extensive connections throughout the brain (Figure 2) (Jafari, Kolb et al. 2020). A direct, ascending pathway directs auditory stimuli from mechanoreceptor cells in the ear to the auditory cortex for conscious perception via the inferior colliculus. An additional descending pathway carries feedback from the temporal lobe to regions mediating auditory sensation as one form of adaptive regulation. A third, indirect pathway connects sensory input from the inner ear to the endocrine system, autonomic nervous system, and limbic pathways mediating physiological, emotional, and behavioral responses to auditory information. CNS may

alter neural circuits by causing reverberation of activity within these networks after cessation of the noise stimulus (Westman and Walters 1981).

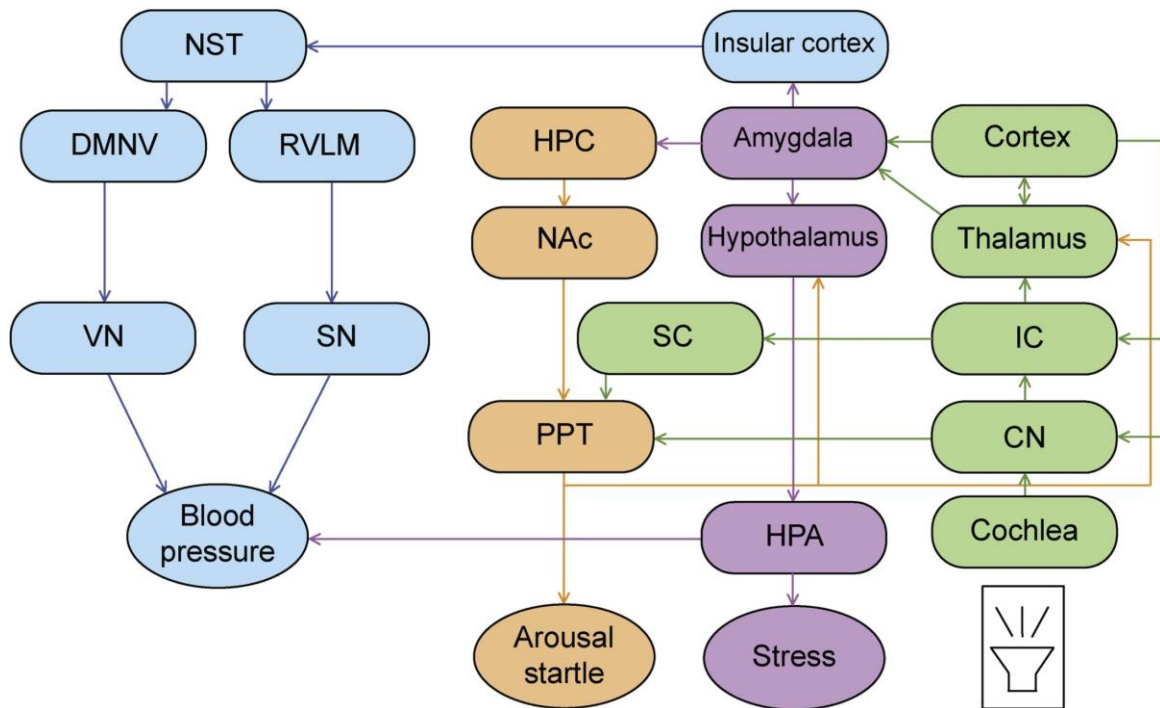


**Figure 2. Auditory system connections to stress systems in the brain.** The auditory perceptual system (green; CN, cochlear nucleus; IC, inferior colliculus; SC, superior colliculus) forms connections with the limbic system and stress-mediating networks (purple) to influence arousal and startle (orange; NAc, nucleus accumbens; PPT, pedunculopontine tegmental nucleus). These systems interact to regulate blood pressure (blue; NST, nucleus of the solitary tract; DMNV, dorsal motor nucleus of the vagus, RVLM, rostral ventrolateral medulla; VN, vagus nerve; SN, sympathetic nerve) via the insular cortex and HPA-axis. Reprinted with permission from Elsevier Publishers Ltd: *Neuroscience & Biobehavioral Reviews* (Jafari, Z., Kolb, B.E., Mohajerani, H., 2020), copyright 2019.

### **1.1.2. Modeling stress in mice**

Rodents are the most common mammals used in research, with mice widely considered the model organism of choice for animal models of human diseases (Simmons 2008). In addition to their short life cycle, gestation period, lifespan, high breeding efficiency and relatively low cost of use, mice and humans share 99% of their DNA (Rosenthal and Brown 2007). Recent advances in mouse genetic engineering have been used to generate several hundreds of mouse models of disease (Gurumurthy and Lloyd 2019), and transgenic mice are also used to study *in vivo* cortical activity with high temporal and spatial resolution (Xie, Chan et al. 2016, Karimi Abadchi, Nazari-Ahangarkolae et al. 2020).

In 1872, Charles Darwin observed that emotion is preserved among humans and other mammals (Ekman 2009). This observation has been applied to create nonhuman models of emotion and emotion disorders, which can be studied without many of the experimental limitations of human subjects (Campos, Fogaca et al. 2013). Brain imaging in humans shows structural and network-level changes in response to chronic stress similar to those found in rodents, including hyperexcitability of emotion networks and altered brain morphology (Pittenger and Duman 2008, Patel, Kas et al. 2019). When mice are exposed to chronic physical or psychological stressors, they exhibit anxiety-like and depressive behavioural phenotypes which are used as models of human stress-related behavioural pathologies (Fuchs, Czeh et al. 2004, Nollet, Le Guisquet et al. 2013).

## **1.2. The hippocampal-cortical-amygdala network**

Because chronic stress is linked to behavioural pathologies, it is important to understand its correlated network-level alterations in the brain. When brain regions are chronically excited for a prolonged period, as is the case during CNS, excited regions may be slow or unable to turn off when the unwanted stimulus stops (Jacinto, Reis et al. 2013). This hyperexcitability may be due to structural remodeling of stress networks in the brain due to stress-induced changes in CORT levels, GRs, neurotransmitters, genetics, and epigenetic factors (Patel, Kas et al. 2019).

Alterations in connectivity between cortical regions have been documented in chronically stressed individuals (Hultman, Ulrich et al. 2018), and a functional pathway between the ventral hippocampus (vHPC), medial prefrontal cortex (mPFC), and basolateral amygdala (BLA) has been shown to mediate stress perception and response in humans and rodents (Orem, Wheelock et al. 2019, Diaz and Lin 2020). The intersection of these two findings lies in a network between the vHPC, BLA, and the entire neocortex: the hippocampal-cortical-amygdala (HCA) network (Stein, Wiedholz et al. 2007, Supcun, Ghadiri et al. 2012). Electrophysiological recordings within regions of the HCA network suggest that temporal synchrony is mediated by theta (4-12Hz), slow gamma (40-70Hz), and fast gamma (70-120Hz) oscillations within local field potential (LFP) recordings (Buzsaki 2002), which measure the net subthreshold activity within some radius of a recording electrode. Structural remodeling and alterations in excitability and synchrony between HCA regions may underlie stress-induced behavioral and cognitive alterations (McEwen 2006, Boyle 2013, Sharp 2017).

### **1.2.1. The ventral hippocampus**

The hippocampal formation was divided into three fields, CA1, CA2, and CA3 (Figure 3) by Lorente de N6 which have been shown to have distinct intrinsic and extrinsic connectivity for different functions in memory and emotion (Witter 2012). The vHPC CA1 pyramidal neurons provide the main excitatory output to the mPFC, have indirect inhibitory projections to the hypothalamus, and form bidirectional connections with the BLA (Godoy, Rossignoli et al. 2018). The vHPC forms these connections with the BLA and neocortex to mediate stress memory, perception, and response by contributing contextual information about a stressor to a functional circuit between the neocortex and BLA (Godsil, Kiss et al. 2013). The vHPC also provides inhibitory control over the HPA-axis via indirect connections to the hypothalamus, providing evidence for its role in mediating the chronic and acute stress response (Herman, Tasker et al. 2002, Pittenger and Duman 2008).

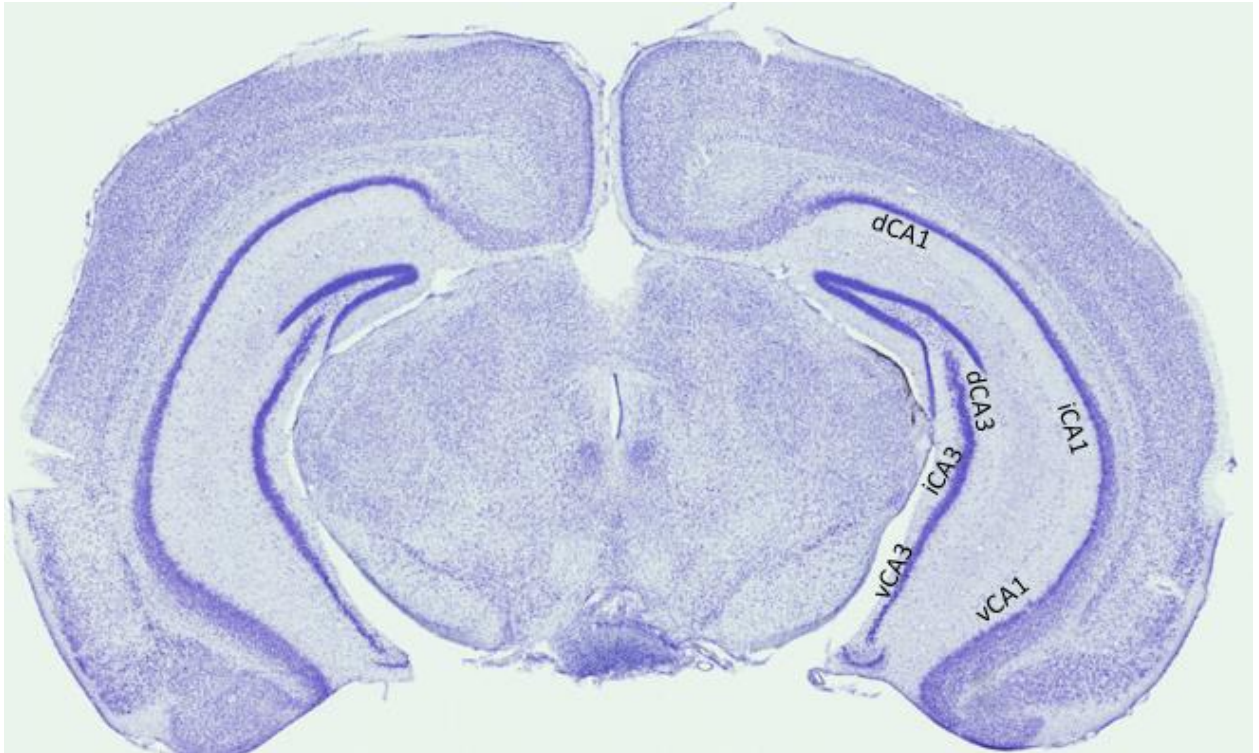


**Figure 3: The mouse hippocampus.** The mouse hippocampus is conventionally divided into three functionally distinct cell layers with differences in intrinsic and extrinsic connectivity. Each cell layer is further subdivided into dorsal (d), intermediate (i), and ventral (v) subregions with unique functional roles. Ventral CA1 (vCA1) forms connections between the cortex and BLA to mediate adaptations to chronic and acute stress.

Hippocampal local field potential (LFP) recording exhibits patterns of theta activity and sharp-wave ripples (SWRs). Theta activity is essential for learning and memory by temporally organizing intrinsic and extrinsic neural connections and modulating synaptic weights for neural plasticity (Buzsaki 2002, Montgomery, Betancur et al. 2009), and theta oscillations originating in the hippocampus have been shown to mediate the precise timing of neural activity required for fast-acting long-term potentiation (Clouter, Shapiro et al. 2017). Behavioural correlates of hippocampal theta activity have been established, and disrupted theta rhythms have been shown to correlate to behavioural deficits (Winson

and Abzug 1978, Soltani Zangbar, Ghadiri et al. 2020). Theta activity in the vHPC has a high coherence with activity in the BLA and mPFC in control subjects, but is susceptible to a loss of synchrony when exposed to stressors (Yang and Wang 2017).

SWRs are synchronous hippocampal spiking motifs occurring at 30-200 events/min and are triggered in CA1 by excitatory output from CA3 (Buzsaki 2015, Jiang, Liu et al. 2018). SWRs typically occur during sleep and quiet wakefulness and may affect endocrine stress responses via connections to the hypothalamus (Buzsaki 2015). Selective disruption of SWRs has been shown to impair memory consolidation and recall important for behavioural functioning (Joo and Frank 2018).

The HPC was also one of the first brain regions to be recognized as a target for glucocorticoids, which have been shown to affect hippocampal morphology (McEwen 2007). Stress-induced hippocampal atrophy is also an established marker in anxiety and depressive phenotypes following chronic stress exposure (Jafari, Kolb et al. 2018, Belleau, Treadway et al. 2019).

### **1.2.2. The neocortex**

The neocortex comprises the most recent evolutionary addition to the mammalian brain. The cortex is a six-layer structure forming the outermost dorsal surface of the brain (Figure 4), and is essential for higher-order functions including cognition, sensory processing, and planning and execution of motor movements (Jawabri and Sharma 2020).

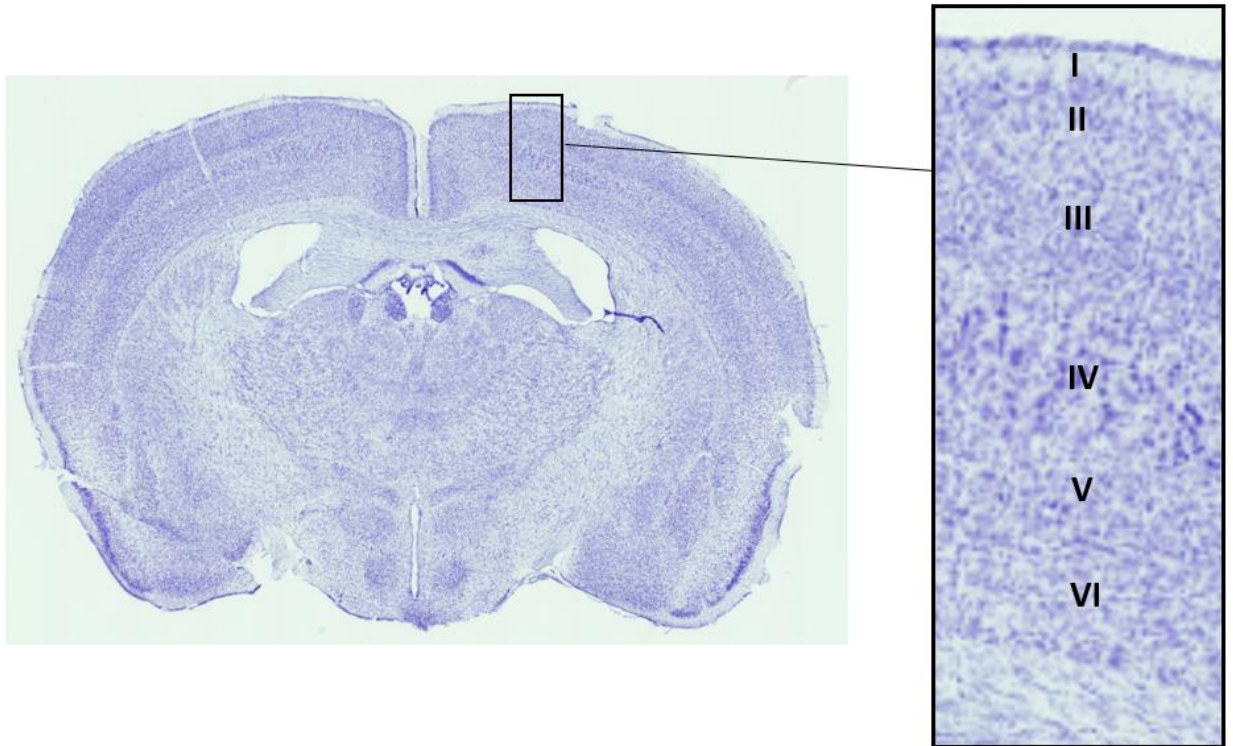


**Figure 4: the mouse neocortex.** Cresyl violet-stained section showing six distinct cell layers in the mouse neocortex.

The mPFC's role in stress adaptation has been studied in a functional network including the vHPC and BLA. The mPFC forms reciprocal connections within this network for top-down regulation of stressful stimulus perception and emotional behaviour, and it also influences the HPA-axis via indirect connections to the hypothalamus (Godoy, Rossignoli et al. 2018). Functional magnetic resonance imaging in humans has established the mPFC as a focal point for processing emotional stimuli (Riga, Matos et al. 2014), and stress-induced atrophy and dysregulation of its circuitry precipitates psychological conditions including anxiety and depression (Pittenger and Duman 2008, Patel, Kas et al. 2019, Liu, Zhang et al. 2020).

Although the mPFC has been studied in the context of emotional behaviour, less is known about the effects of stress on entire cortical networks and their correlation to lower brain regions and behaviour. One method for studying cortical networks is imaging spontaneous activity, which reveals a default mode network of spatial and temporal brain activity in the absence of sensory experience and motor behaviour. Imaging in animal models can record patterns of neural activity with a high temporal and spatial resolution and has been used to map functional areas of the neocortex (Mohajerani, Chan et al. 2013, McGirr, LeDue et al. 2017) . Patterns of visual, auditory, and somatosensory stimulation are present in spontaneous recordings, which may echo patterns of activation within the vHPC and mPFC (Mohajerani, Chan et al. 2013). Alterations of neural motifs in the default mode network may be related to psychiatric illness and the anxiety and depressive behavioural symptoms of chronic stress (Menon 2011).

A key regulator of the stress response in cortical networks is glutamate (Glu), the main excitatory neurotransmitter in the brain, and its N-methyl-D-aspartate (NMDA) and  $\alpha$ -amino-3-hydroxy-5-methyl-4-isoxazolepropionic acid (AMPA) receptors (Patel, Kas et al. 2019). Glu works synergistically with glucocorticoids to produce adaptive behavioural and network-level responses to acute stressors (Herman, McKlveen et al. 2016), but chronic stress alters levels of Glu, NMDARs, and AMPARs. Widefield optical imaging can be used to visualize changes in cortical Glu, and studies have implicated excess neural excitation as a possible cause of stress-induced behavioural symptoms (McGirr, LeDue et al. 2017, Dunkley, Wong et al. 2018).

### **1.2.3. The basolateral amygdala**

The amygdala is an almond-shaped structure within the limbic system that is broadly divided into three subnuclei: the basolateral nucleus, corticomедial nucleus, and central nucleus, which receive and process emotional input (Patel, Kas et al. 2019). The basolateral nucleus is further subdivided into the lateral, basal (BLA), and basomedial nuclei (Figure 5), each with distinct and overlapping connectivity and behavioural functions (Yang and Wang 2017). Ablation and stimulation experiments demonstrate that these nuclei have distinct influences in behaviour (Kaada 1972), and that the BLA is particularly important for processing psychological stressors, consolidating stressful memories, and eliciting emotional and motivational responses to stressful stimuli (McDonald 1998, Godoy, Rossignoli et al. 2018). Studies have implicated the BLA as crucial to the development of chronic stress-related behavioural pathologies including anxiety and depression (Patel, Kas et al. 2019).

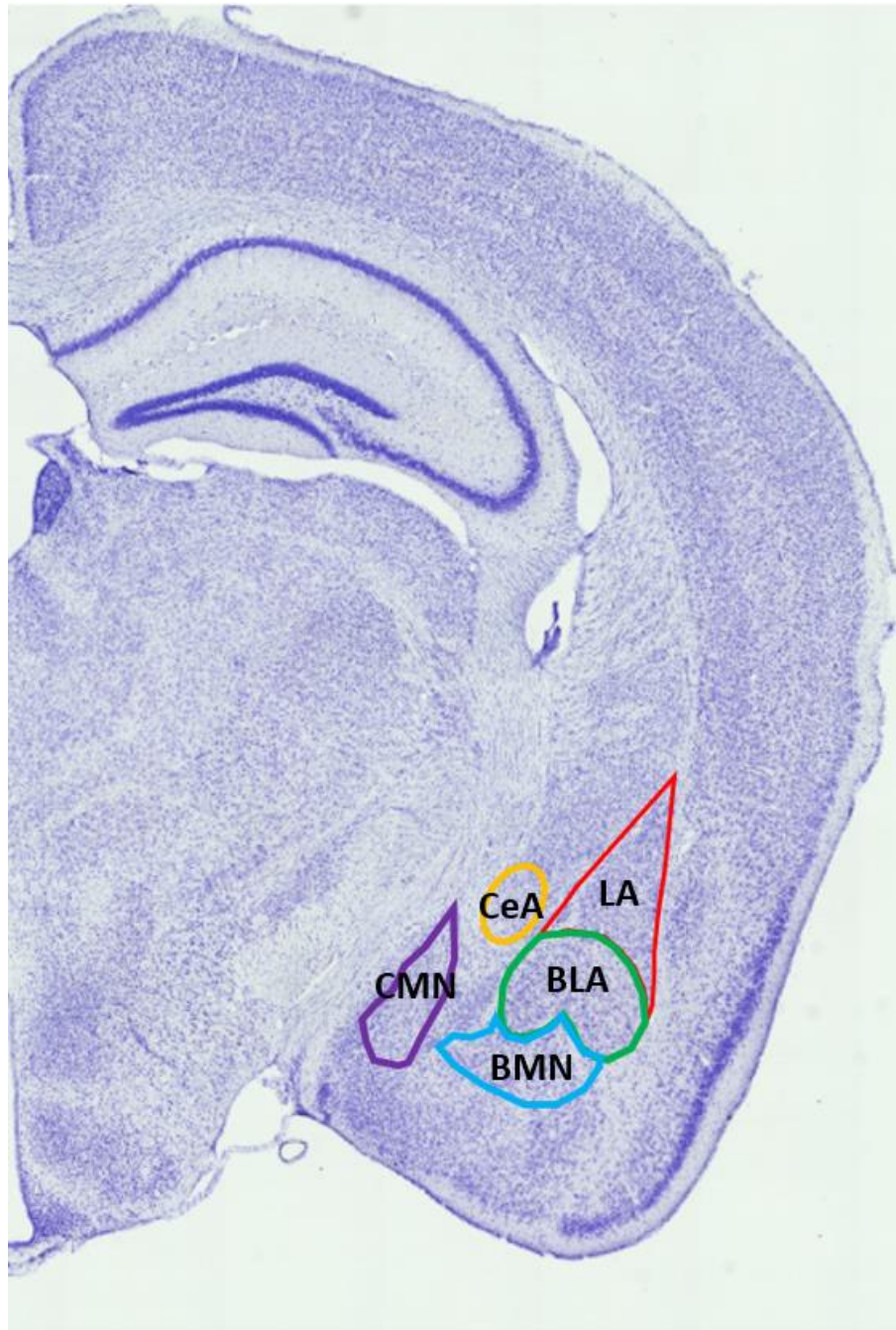


**Figure 5: The mouse amygdala.** The amygdala is broadly divided into the central nucleus (CeA, orange), the corticomedial nucleus (CMN, purple), and the basolateral nucleus including the lateral amygdala (LA, red), basal nucleus (BLA, green), and basomedial nucleus (BMN, blue).

The BLA consists of 80-90% excitatory projection neurons and 10-20% inhibitory interneurons (Liu, Zhang et al. 2020). Its connections to the vHPC and mPFC contribute excitatory and inhibitory input, and excitatory projections from the BLA to the hypothalamus increase HPA-axis activity (Boyle 2013, Jacinto, Reis et al. 2013). BLA LFP signatures include theta oscillations, which are synchronous with theta activity in the vHPC and mPFC of healthy subjects, and slow and fast gamma oscillations, whose power and synchrony may correlate to fear behaviour in response to stressors (Stujenske, Likhtik et al. 2014).

Histological studies of stress-induced amygdala volumetric changes provide inconsistent results. Some chronic stress experiments report hypertrophy within the amygdala (Pittenger and Duman 2008, Hoffman, Parga et al. 2015), while others show amygdala atrophy (Hamilton, Siemer et al. 2008, Gilabert-Juan, Castillo-Gomez et al. 2011, Jafari, Kolb et al. 2018). Electrophysiological recordings in chronically stressed rodents, however, tend to show consistent hyperactivity of the BLA in the presence of chronic stressors (Rosenkranz, Venheim et al. 2010, Zhang, Ge et al. 2018).

### **1.3. Theory**

Brain structures forming functional connections with the auditory system mediate adaptations to chronic noise exposure. The ventral hippocampus, basolateral amygdala, and neocortex form functional networks to mediate the perception of stressful stimuli. This network is adaptive in the presence of an acute stressor, allowing an organism to optimally prepare and deal with the source of stress, but may become dysfunctional when exposed to chronic stress.

## **1.4 Rationale**

Chronic noise exposure has been shown to act as a stressor and create an allostatic load corresponding to behavioural pathologies (Westman and Walters 1981, Jafari, Kolb et al. 2018). If the vHPC, neocortex, and BLA mediate these changes, then widefield optical imaging, local field potential recordings, and behavioural observation could be used to identify the neural and behavioural correlates of these changes in response to chronic stress.

## **1.5. Hypotheses**

*Hypothesis I. Chronic noise stress will correlate to neocortical hyperconnectivity and decreased synchrony between BLA and vHPC theta activity.* Prolonged psychological stress and accompanying blood cortisol elevation may be related to excitatory changes in the hippocampal-neocortical-amygdala network (McEwen 2017). This possibility will be quantified by recording electrical and chemical signals in structures of the HCA-network.

*Hypothesis II. Chronic noise stress will correlate to altered behaviour.* This possibility will be tested using concurrent recordings of pupil activity during head-fixed recordings of brain activity.

*Hypothesis III. Chronic noise stress will correlate to altered brain morphology including shrunk hippocampal, cortical, and whole brain volume and amygdala hypertrophy.* A decrease in hippocampal volume and cell density has been shown to accompany chronic stress and anxiety-like behaviours (Jafari, Kolb et al. 2018), and chronic stress has been shown to alter activity and morphology of brain regions involved in the mediation of

emotional reactions to auditory stimuli (Haines, Stansfeld et al. 2001, Alimohammadi, Ahmadi Kanrash et al. 2018). Changes will be quantified by using histological methods to analyze changes in brain morphology.

## 2. Chronic noise stress experiment

### 2.1. Introduction to experiment

In order to identify the hippocampal-cortical-amygdala network correlates of chronic stress, widefield glutamate imaging of the neocortex was used with simultaneous LFP recordings in the BLA and vHPC. Each recording was divided into two segments: the first measured spontaneous brain activity, and the second recorded activity during noise exposure. Pupil fluctuations were also filmed during recordings to analyze the behavioural correlates of chronic stress and brain network activity. This recording paradigm was used to compare baseline brain activity with activity following a chronic noise intervention. The brain was then mapped using sensory evoked stimuli to identify the cortical regions to be used for correlational analysis. Finally, histological measures were used to determine stress-related morphological alterations in the hippocampus, neocortex, and amygdala (Figure 6).

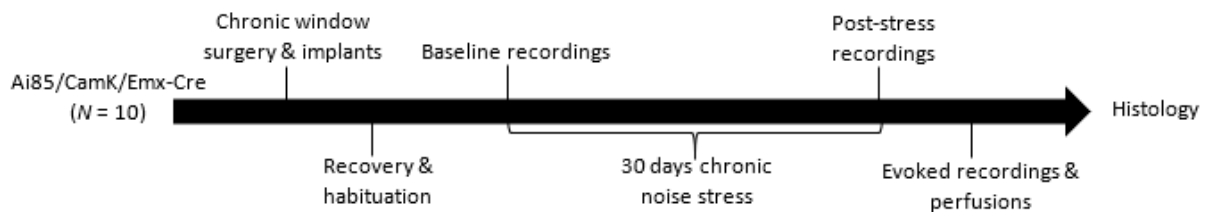


**Figure 6. Overview of chronic noise experiments.** Ten mice were implanted with chronic windows and electrodes, then separated evenly into stress and control groups. The first recordings were taken after surgical recovery and habituation to head-fixation. Stress animals were exposed to chronic stress for 30 days, then a second set of recordings were taken in all animals. Evoked recordings were taken within one week of the second recordings, then animals were perfused and brains were extracted for histology.

## 2.2. Glutamate imaging

Widefield glutamate (Glu) imaging uses modified glutamate receptors to visualize cortical activity and connectivity with a high temporal and spatial resolution. While calcium imaging is widely used to map cortical neuronal activity, its temporal resolution (seconds) can be limiting and it is largely a measure of suprathreshold activity (Tian, Hires et al. 2009, Xie, Chan et al. 2016, Afrashteh, Inayat et al. 2020, Bermudez-Contreras, Gomez-Palacio et al. 2020, Karimi Abadchi, Nazari-Ahangarkolaee et al. 2020). Voltage-sensitive dye (VSD) has a higher temporal resolution (~10ms rise), but the organic dye cannot be used for chronic experiments (Devonshire 2014, Xie, Chan et al. 2016). Glu imaging provides a solution to each of these limitations, as it can be genetically encoded and has a ~1ms rise and ~40ms decay resolution (Marvin, Borghuis et al. 2013).

The single-wavelength ionotropic Glu reporter (iGluSnFR) was constructed from *E. Coli* *gltI*, a gene that encodes the periplasmic component of a glutamate transporter, and cpGFP, a green fluorescent protein. Its high temporal and spatial resolution for chronic imaging is achieved by its single-wavelength fluorescent property, allowing its corresponding imaging signal to be unambiguously assigned to Glu (Marvin, Borghuis et al. 2013). Cortical maps imaged with iGluSnFR have also been validated as consistent with maps determined with calcium or VSD imaging (Xie, Chan et al. 2016, McGirr, LeDue et al. 2017).

It has been shown that Glu imaging mainly is representative of presynaptic subthreshold activity (Marvin, Borghuis et al. 2013), making it a good candidate for correlative LFP analysis. Glu imaging also provides a temporal resolution up to the alpha band (8-12Hz),

making it well suited for correlation studies with LFP activity within and below this range. Finally, because Glu is implicated in anxiety-like and depressive phenotypes, imaging its activity in the neocortex has potential utility in understanding these chronic stress-induced behavioural symptoms (Xie, Chan et al. 2016).

## **2.3. Methods**

### **2.3.1. Animals**

20 Ai85/CamK/Emx-Cre mice (10 female, 10 male) expressing the extracellular fluorescent glutamate reporter iGluSnFR in all six cortical layers, weighing 25-35g, and aged 10-11 months from the Canadian Centre for Behavioural Neuroscience vivarium were used. Ten animals did not survive surgery due to excessive ageing and were excluded from subsequent recordings and analysis. The remaining ten animals (four female, six male) were used for experiments. Animals were given access to food and water ad libitum and singly housed in standard cages on a 12h:12h light/dark cycle from 7:30am to 7:30pm in a temperature-controlled room at 21°C. Animals were initially housed in groups of 2-3 with littermates after weaning. After the first surgery they were singly housed to minimize the risk of damage to head implants. Recordings were taken during the light phase at the same time of day for each animal. All procedures were approved by the University of Lethbridge Animal Care Committee in accordance with the Canadian Council of Animal Care guidelines.

### **2.3.2. Chronic noise stress group**

Animals assigned to the stress group ( $N = 5$ ; 3 male, 2 female) were transferred in their home cages to a separate testing room and exposed to an 8hr recording (8:00am – 4:00pm) of broadband traffic noise daily for 30 days. The CNS recording was emitted

from a speaker which maintained a 75dB SPL in the home cages (min = 70.8 dB; max = 79.1 dB; peak = 81.3 dB; frequency spectrum = 65–9200 Hz), which has been shown to elicit a chronic stress response in mice without causing hearing damage (Jafari, Kolb et al. 2018). The SPL was monitored daily inside an empty home cage (Tektronix RM3000, Digital Phosphor Oscilloscope). Animals were returned to main housing at 4:00 pm each day.

### **2.3.3. Control group**

Animals assigned to the control group ( $N=5$ ; 3 male, 2 female) were transferred in their home cages to a separate testing room across from the stress group. A silent speaker was placed in the same proximity to the home cages as the stress group, and the control mice were left undisturbed for 8hrs per day (8:00am – 4:00pm) for 30 days. Control animals were returned to main housing at 4:00 pm each day.

### **2.3.4. Electrode fabrication**

Electrodes were fabricated to record EMG signals and LFP activity in the vHPC and BLA. The EMG electrode was fabricated from a multi-stranded, Teflon-coated stainless-steel wire (A-M Systems catalogue #793500). The wire was trimmed to 2cm with a razor blade and soldered to a gold pin (A-M Systems catalogue #520200) for implantation in the animal's neck muscle. The vHPC electrodes were fabricated in the same fashion using a 127 $\mu$ m stainless-steel wire (A-M Systems catalogue #791500).

BLA electrodes were fabricated from sharpened Epoxy-insulated stainless-steel (254 $\mu$ m) electrodes (A-M Systems catalogue #571000). Electrode tips were gold-plated to decrease impedance from 8M $\Omega$  to 250-300K $\Omega$  using an isolated pulse stimulator (A-M Systems) to inject current and an impedance meter (Bak Electronics Inc.) to monitor impedance.

Electrodes were then trimmed to 6mm and soldered to a gold pin. These electrodes were chosen for BLA recordings because they were rigid enough to reach the BLA by stereotaxic coordinates without bending as they were lowered into the brain.

### **2.3.5. Surgical procedure**

Animals were implanted at ten months with single electrodes in the left BLA and CA1 region of the vHPC, and a large, unilateral section of the skull above the right hemisphere was exposed for imaging using aseptic methods (Figure 7). Laterality in neocortical mesoscale optical imaging and HPC and BLA LFP has not been found in mice, so the side of implants were chosen for recording convenience. Buprenorphine (0.02mg/mL) was administered for analgesia 30 mins prior to surgery, and 1-2% isoflurane was vaporized in oxygen at a flow rate of 1mL/min for anesthesia. Body temperature was kept at  $37 \pm 0.5^{\circ}\text{C}$  throughout the procedure using a feedback loop heating pad. 0.4mL Lidocaine with epinephrine (20mg/mL) was injected subcutaneously over the skull 10 mins prior to the beginning of the procedure. A reference electrode was first placed on the cerebellar surface, and then a custom assembled electrode was lowered to the CA1 region of the vHPC with a stereotaxic apparatus (RC -3.2; ML -3.2; DV -3.4). The vHPC electrode was guided by a simultaneous live LFP recording with audio monitoring (Grass Instrument Co.) and fixed to the skull when it showed consistent theta activity within 0.1mm of the target DV coordinates. A custom sharp electrode was implanted in the BLA using stereotaxic coordinates (RC -1.1; ML -2.4; DV -4.7). All electrodes were fixed with tissue glue and dental acrylic. A 6.5 x 6 mm window located +2.8 to -3.7 mm from bregma and 6 mm lateral from midline was left exposed over the skull, and temporal muscle within the window was removed. A headplate was fixed to the

skull surrounding the window with Metabond. Animals were monitored in a temperature-controlled surgical recovery cabinet and administered 0.05mL Baytril (1mg/mL in sterile saline) and 0.05mL Metacam (5mg/mL) every 24hrs for the following 3-5 days.

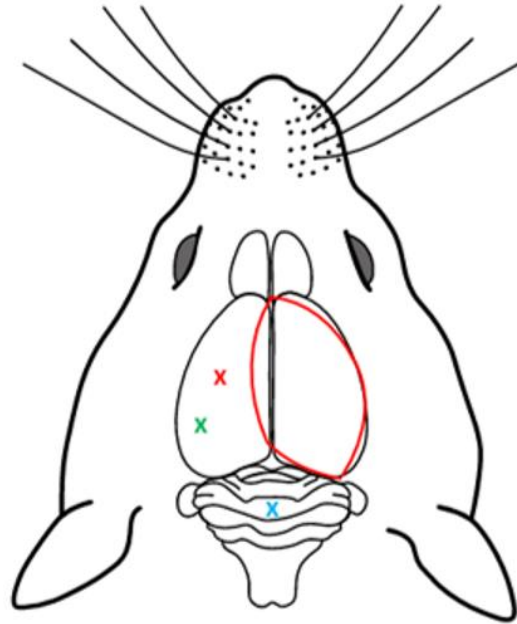


**Figure 7. Schematic of chronic surgical implants.** A large, unilateral window was implanted over the right hemisphere (red oval) and electrodes were implanted in the basolateral amygdala (red x) and ventral hippocampus (green x). A reference electrode was placed in the cerebellar surface (blue x). This figure was created using an image from SciDraw, a free repository of scientific drawings.

### 2.3.6. Recordings

Animals were habituated to head-fixation daily for one week prior to chronic recordings (Figure 8). Each recording consisted of 15 mins of quiet, spontaneous activity followed by 15 mins of spontaneous activity with traffic noise playing in the recording chamber. A microscope composed of front-to-front video lenses (8.8x8.6 mm, 67 $\mu$ m/pixel) was used for imaging. A 470nm LED was used to excite iGluSnFR, and fluorescence was filtered using a 530nm bandpass filter. Cortical glutamate activity was captured in 12-bit format at 150Hz (6.67ms) temporal resolution for a total of 135,000 frames per 15 min recording

segment using a CCD camera (1M60 Pantera, Dalsa) and XCAP 3.8 imaging software (EPIX, Inc.). LFP activity recorded at 20 kHz with an Axon Instruments data acquisition system, amplified at x1000, and filtered from 0.1 to 10,000 Hz with a Grass P5 amplifier. A camera (RaspberryPi 3B) was used to capture pupil fluctuations and behaviour during all recording segments. Two recordings were taken per animals for analysis.

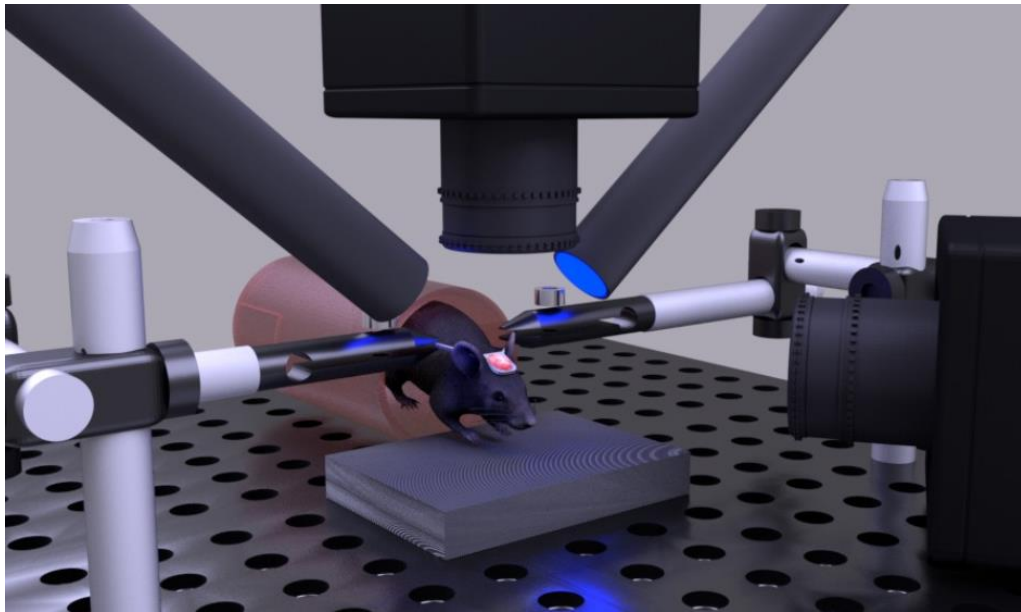


**Figure 8: Chronic head-fixed recordings schematic.** Mice were head-fixed for recordings and blue LEDs were used to excite iGluSnFR recordings. An imaging camera (top) was used to capture cortical activity and a behaviour camera (right) was used to collect pupil activity data.

#### *2.3.6.1. Sensory evoked mapping*

Immediately prior to perfusion, animals were anaesthetized with isoflurane for evoked mapping of sensory ROIs. Five sensory areas were stimulated for recording: forelimb, hindlimb, auditory, visual, and whisker. Electrodes were inserted subcutaneously into the left forelimb and hindlimb (contralateral the cranial window) of each animal and were

stimulated using a 0.2mA pulse for one second. Auditory stimulation involved a one second, 80dB click played through a speaker placed to the ear contralateral the cranial window. Visual stimulation used a one second pulse of 550nm light directed at each animal's left eye. All whiskers except C2 were trimmed and a piezoelectric bending actuator was positioned to stimulate the remaining C2 at 5Hz for one second. Cortical ROIs (5x5 pixels) were identified in ImageJ using the Shawn Own plugin to compare the normalized difference of ten evoked trials to the average of ten stimulus free trials within the 1000 frames surrounding stimulus onset. An additional 14 ROIs were derived from sensory evoked responses in relation to their stereotaxic coordinates from bregma, including secondary motor/anterior cingulate (aM2/AC), posterior secondary motor (pM2), retrosplenium (RS), secondary barrel sensory (BC C2 S2), parietal association area (ptA), medial secondary visual (V2MM and V2LM), lateral secondary visual sensory (V2L), primary shoulder/neck sensory (S1J S1), secondary hindlimb sensory (HLS2A), secondary forelimb sensory (FL S2), barrel motor (mBC), forelimb motor (mFL), and hindlimb motor (mHL) (Figure 9).

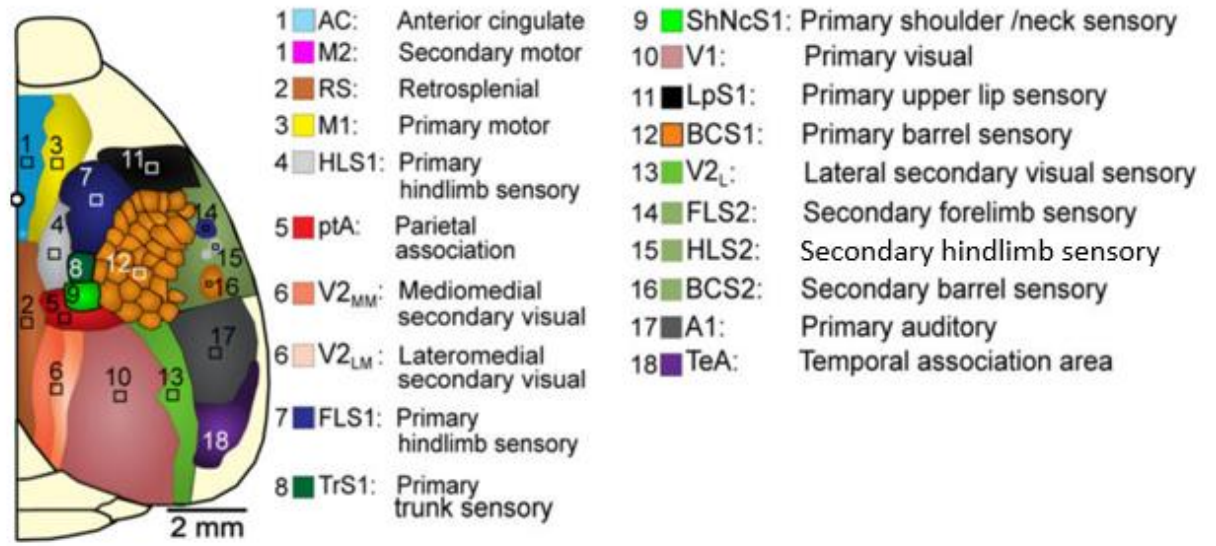


**Figure 9: Sensory evoked map of the mouse neocortex.** Schematic of sensory areas determined with evoked stimulation and coordinates from bregma. Reprinted with permission from Macmillan Publishers Ltd: *Nature* (Mohajerani, Chan et al. 2013), copyright (2013).

### 2.3.6.2. Widefield imaging analysis

Widefield imaging fluorescent signals were first preprocessed using a custom MATLAB script (Figure 10). A unique image mask created in ImageJ was applied to each recording, and the time series of each pixel was filtered using a zero-phase highpass Chebyshev filter ( $> 0.2\text{Hz}$ ) of order 3. Next, all frames were averaged to determine the baseline signal ( $F_0$ ). The difference between  $F_0$  and the filtered signal ( $F$ ) was used to compute changes in fluorescence ( $\Delta F$ ) by the following equation:

$$\Delta F = \frac{(F - F_0)}{F_0} \times 100$$

Preprocessed spontaneous imaging data were used to create 19 x 19 correlation matrices based on 5 x 5 pixel ROIs determined with sensory evoked mapping and coordinates from

bregma. Zero-lag correlations of spontaneous activity were first computed for each animal, then combined into the overall average correlation of each ROI. Significance between ROIs for each recording condition were computed using a two-sample t-test. Because data interpretation was concerned only with the change in the correlations of ROIs under the two conditions, and the number of tests for both conditions were the same, Bonferroni corrections were not used.

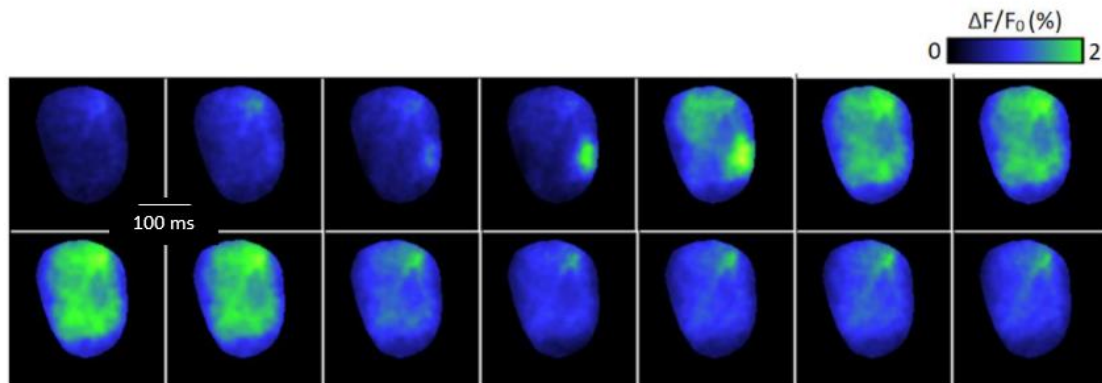


**Figure 10: Example montage of evoked cortical activity.** Example illustrate auditory evoked iGluSnFR cortical response in a control animal to a tone stimuli.

### 2.3.6.3 Electrophysiology analysis

LFP signals were first downsampled to 1 kHz for analysis with custom MATLAB scripts (Figure 11). To compute vHPC-BLA theta synchrony, a bandpass filter for 4-10.5Hz was first applied to each signal. The amplitude of the Hilbert transform of the signal was then computed. A 10 min window beginning after the first 3 mins of each recording segment was considered for analysis. A 1 sec window of activity that moved at 20 ms increments was applied to the entire 10 min of the Hilbert phase signal. This window was then used

to compute the minimum lag between signals that represented peaks in correlation. A two-sample t-test was used to determine significance between recording conditions. Significance values were set at  $p = 0.025$  based on a Bonferroni correction.

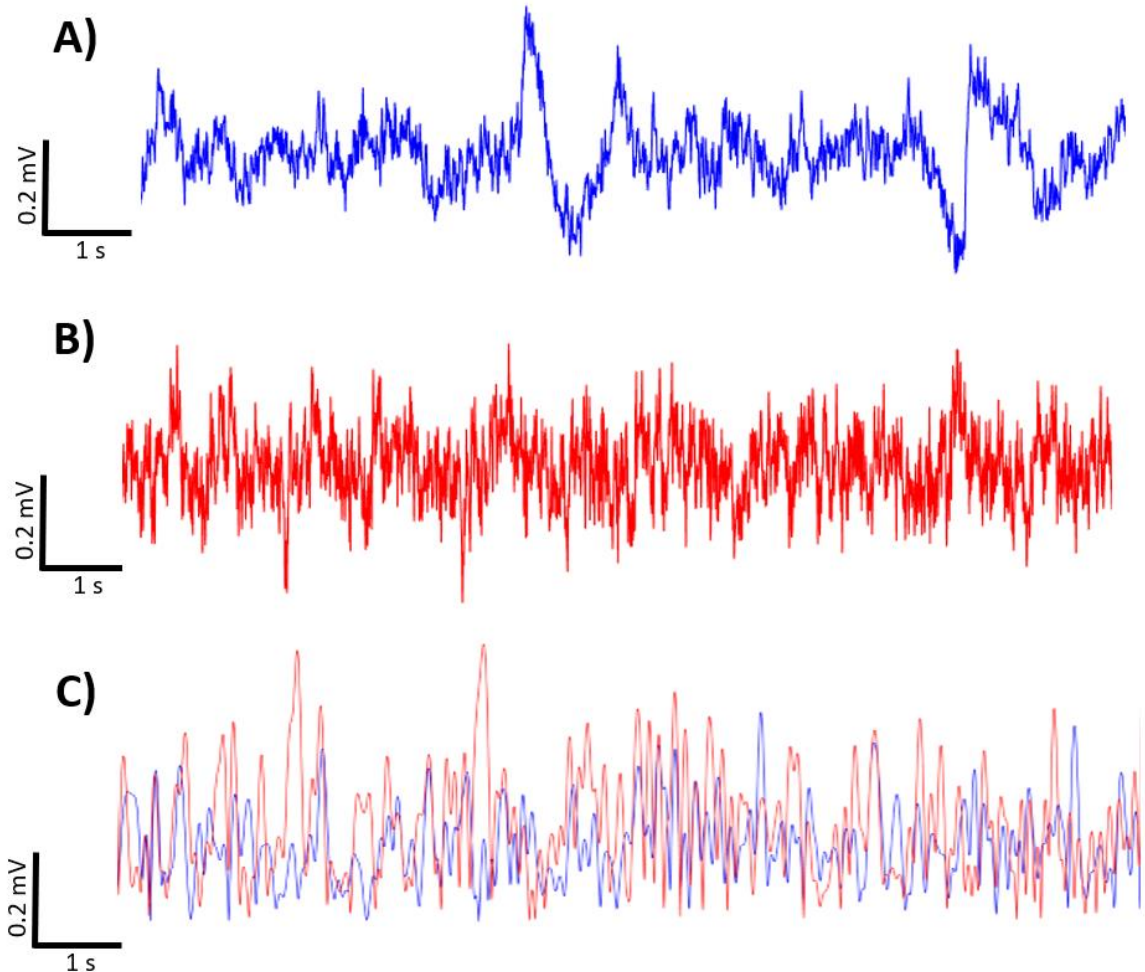


**Figure 11: Example LFP theta signals and leading/lagging analysis.** A) Raw LFP signal recorded in vHPC. B) Raw LFP signal recorded in BLA. C) Filtered vHPC LFP (blue) and filtered BLA (red) signals used for leading/lagging analysis.

#### 2.3.6.5. Behavioural analysis

Pupil fluctuation data were extracted using facemap 0.2.0, a Python graphical user interface (GUI) for processing rodent behavioural videos. ROIs were defined for each

recording segment surrounding the pupil and eye of each mouse. Frames with blinking or movement were removed from final analysis. All measurements were first converted from pixels to mm. The derivative of pupil area was computed for each animal to determine the speed of pupil fluctuation, then the mean of each recording segment was computed for all animals in each group. A t-test was used to determine significance between groups and recording conditions.

### **2.3.7. Histology and morphological analysis**

While animals were under anesthesia following evoked mapping, an overdose of Euthansol was injected IP and animals were perfused with 20mL of 1% PBS through the left ventricle followed by 20mL of 4% PFA in 1% PBS. Brains were removed, post-fixed overnight in 4% PFA, then transferred to a 30% sucrose in 1% PBS solution for cryoprotection. After 48 hours, brains were sectioned coronally at 40 $\mu$ m using a sliding microtome with blockface imaging. Every third slice was collected for morphological analysis, mounted on Superfrost Plus slides (VWR), and stained with cresyl violet. A two-sample t-test was used to compare stress and control group brain morphology using IBM SPSS Statistics 26.

All slides within -0.82mm to -3.88mm AP from bregma were also collected and stained with cresyl violet to confirm the locations of BLA and vHPC electrodes (Figure 12 - A, B). Additionally, every tenth section was collected, mounted with vectashield (Vector Labs) mounting medium, and fluorescently scanned to ensure iGluSnFR expression through all six cortical layers (Figure 12 - C). All slides were scanned and analyzed using NDP view2 (Hamamatsu Photonics Japan).

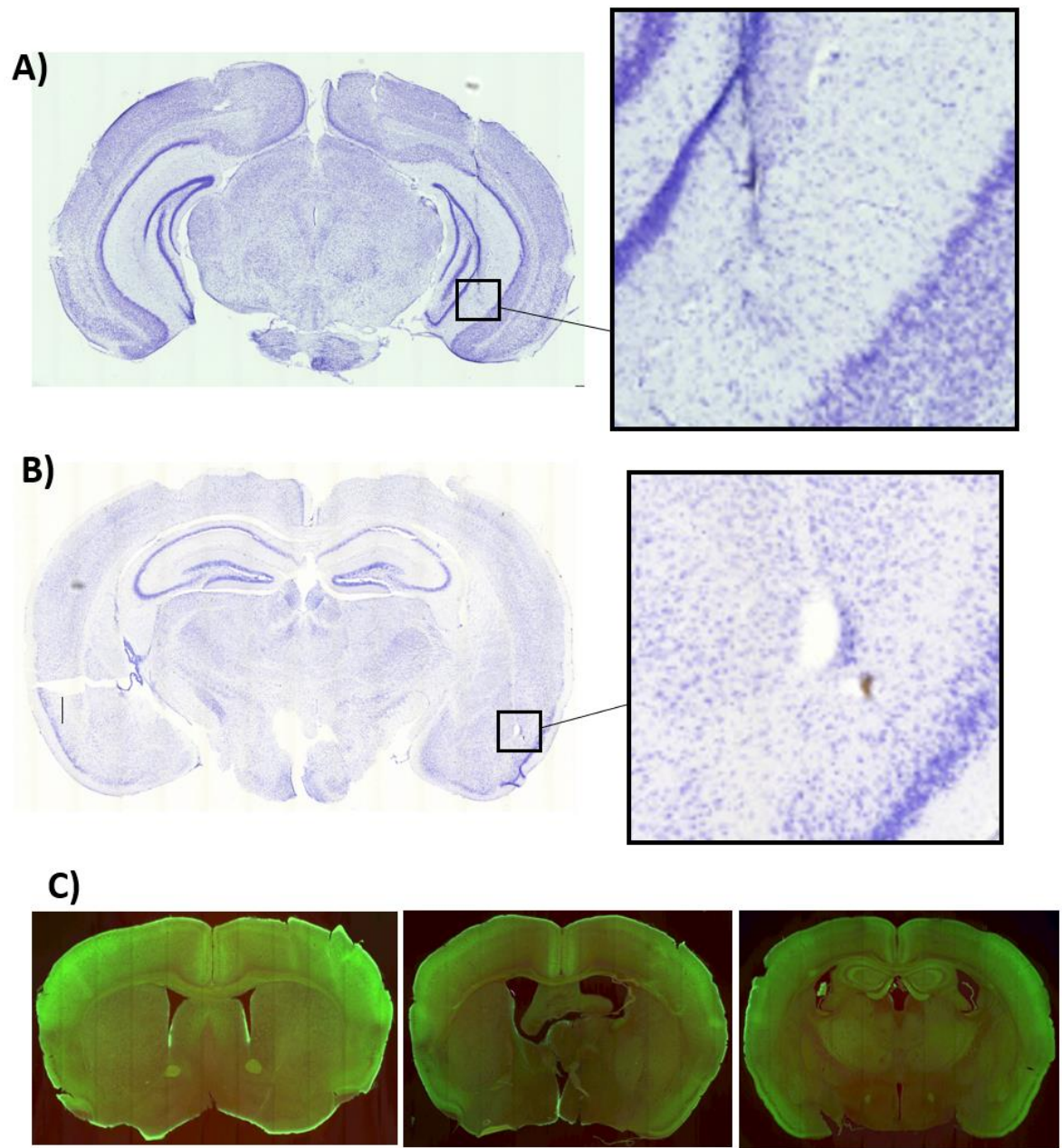


**Figure 12: Histology for electrodes and imaging.** A) Cresyl violet stained section showing a lesion created with the vHPC electrode to demonstrate accurate implantation following experiments. B) Cresyl violet stained section showing a lesion created with the BLA electrode to demonstrate accurate implantation following experiments. C) Fluorescent image of iGluSnFR in all cortical layers.

Brain volume was estimated from 83 ( $\pm 1$ ) cresyl violet stained sections (3 mm to – 8 mm from bregma) for each animal (Figure 13-A). The outline of each slice was first traced to obtain its area, then the sum of areas for each brain was multiplied by slice thickness (0.04 mm) and the sampling interval (3) (Paxinos and Franklin 2001):

$$Volume (mm^3) = \sum areas (mm^2) \times slice\ thickness (mm) \times sampling\ interval$$

Dorsal and ventral hippocampal volume was estimated from 28 ( $\pm 1$ ) cresyl violet stained sections (-0.94mm to -3.99mm from bregma) for each animal using the above equation (Figure 13 - B). The margins of 13 ( $\pm 2$ ) sections of lateral and basolateral amygdala (-0.70 mm to - 2.18 mm from bregma) were considered for volumetric analysis in the same manner (Figure 13 – C).

Central, lateral, and ventrolateral cortical thickness were measured for one hemisphere in seven cresyl violet stained sections. A straight line was used to measure the distance from the inner to outer edges of the cortex (Figure 13 – D). Sections were collected for analysis at 2.46, 2.22, 1.42, 1.10, 0.50, -0.10, and -0.70 mm AP from bregma.

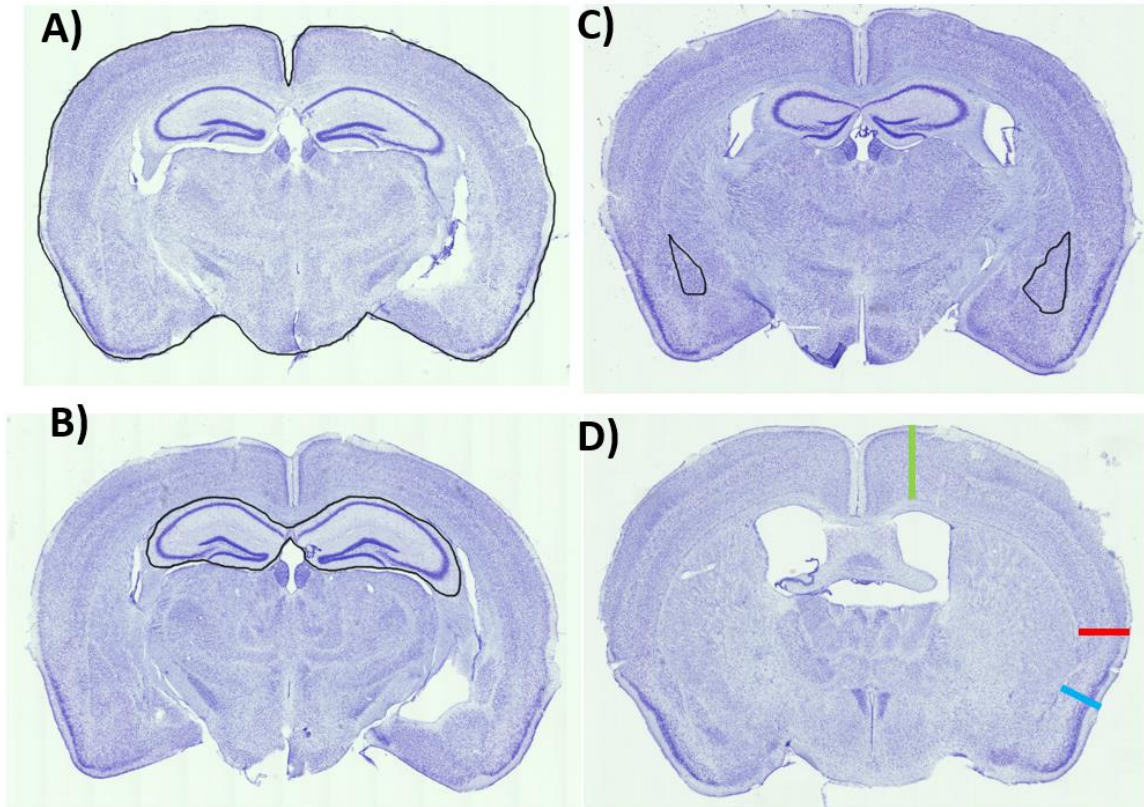


**Figure 13: Rough morphological analysis.** A) Example cresyl violet-stained section of traced contours of the whole brain. B) Example cresyl violet stained section of bilateral hippocampal rough analysis. C) Example cresyl violet section of traced lateral and basolateral regions of the amygdala. D) Central (green) lateral (red) and ventrolateral (blue) measurements of cortical thickness for one cresyl violet-stained section.

## **2.4. Results**

Because the *N*-value was small (5 CNS, 5 control), males and females were pooled for all statistical analysis. There were not enough subjects (2 females per group) to use an ANOVA to determine the effects of sex, group (CNS or control), and recording condition (spontaneous or noise). No statistically significant difference in pupil activity was found between any recording condition in CNS or control animals. Morphological analysis revealed significant shrinkage in the HPC, whole brain volume, and neocortical thickness in CNS animals compared with controls. There was no statistically significant difference between amygdala volume in CNS and control animals. There were significant changes in correlation between four ROI combinations after 30 days CNS between the spontaneous and noise recording conditions that were not found in controls. There were additional changes in correlation for 13 ROI combinations between the baseline spontaneous and post-stress spontaneous recordings in CNS animals that were not found in controls. There were also eight significant changes in correlation between the baseline noise and post-stress noise recordings in CNS animals compared with three significant changes between these conditions in control animals. Analysis of vHPC-BLA theta leading/lagging time revealed a shift towards the BLA leading in the post-stress spontaneous recording condition in CNS animals that was significantly different from all other recording conditions in CNS and control animals.

### **2.4.1. Pupil activity**

Pupil activity was recorded for each 15 min recording segment and analyzed for mean pupil area and its derivative to determine fluctuation speed (Figures 14, 15). A t-test revealed no significance difference in pupil area between the baseline spontaneous and

spontaneous recording after 30 days in controls ( $t(12) = -0.0189, p = 0.9852$ ) or between the baseline noise and noise recording after 30 days in controls ( $t(16) = -0.3281, p = 0.7471$ ). There was also no significant difference in pupil area between the baseline spontaneous and noise recording conditions for control animals ( $t(9) = -0.4095, p = 0.6917$ ), or between the spontaneous and noise recording conditions after 30 days ( $t(9) = -0.4095, p = 0.6917$ ) after 30 days in control condition). Changes in mean pupil fluctuation speed for control animals were also insignificant between the baseline spontaneous recordings and the spontaneous recordings after 30 days ( $t(10) = 2786, p = 0.9922$ ). There was no significant change in pupil fluctuation between the baseline noise recordings and the noise recordings after 30 days for control animals ( $t(14) = -0.2262, p = 0.8243$ ), or between the baseline spontaneous and baseline noise recording conditions for control animals ( $t(15) = -0.4628, p = 0.6501$ ). There was no significant change between the spontaneous and noise recording conditions after 30 days for control animals ( $t(9) = -0.4095, p = 0.6916$ ).

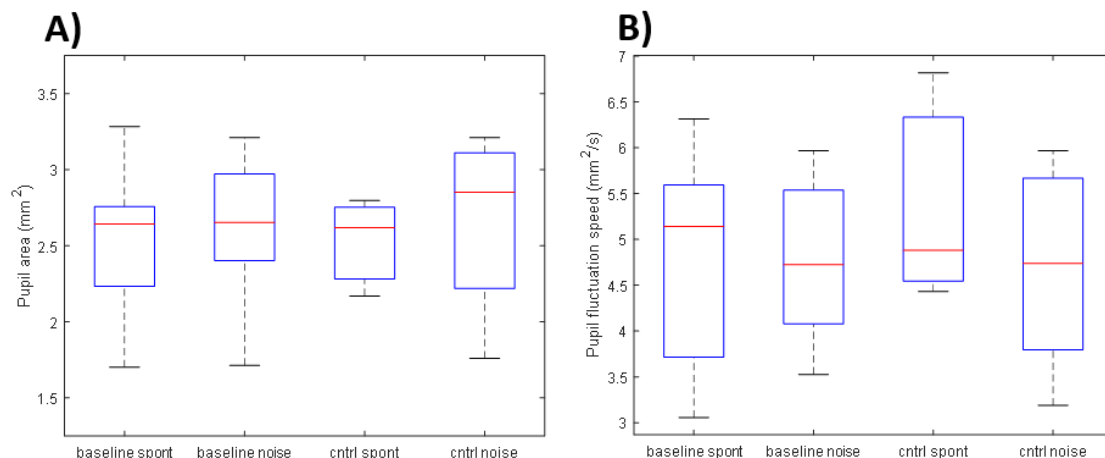


**Figure 14. Pupil activity for control animals during recordings.** A) Pupil area (mm<sup>2</sup>) for control animals in all recording conditions. Red line indicates mean value. B) Pupil fluctuation speed (mm<sup>2</sup>/s) for control animals in all recording conditions.

The CNS animals showed an increase in average pupil area between the pre- and post- CNS spontaneous recording conditions, but a two sample t-test revealed no significance ( $t(13) = -0.8545, p = 0.4083$ ). There was also no significant difference in pupil area between the pre- and post- CNS noise recording conditions ( $t(17) = 0.1237, p = 0.9030$ ). There was no significant change in pupil area between spontaneous and noise baseline conditions ( $t(18) = -0.1383, p = 0.8915$ ), and although there was a decrease in average pupil area from the spontaneous to the noise condition after 30 days CNS, this change was not significant ( $t(9) = 0.9118, p = 0.3856$ ). The mean pupil fluctuation speed did not change significantly in CNS animals between baseline spontaneous and noise recordings ( $t(13) = 0.0073, p = 0.9943$ ) or between spontaneous and noise recordings after 30 days CNS ( $t(4) = 1.7282, p = 0.9958$ ). The pupil fluctuation speed of CNS animals decreased between baseline and 30 days CNS spontaneous recordings, but this change was not significant ( $t(7) = 1.4783, p = 0.1829$ ). The pupil fluctuation speed of CNS animals also decreased between baseline and 30 days CNS noise recordings, but this change was also not significant ( $t(10) = 1.2075, p = 0.1424$ ).

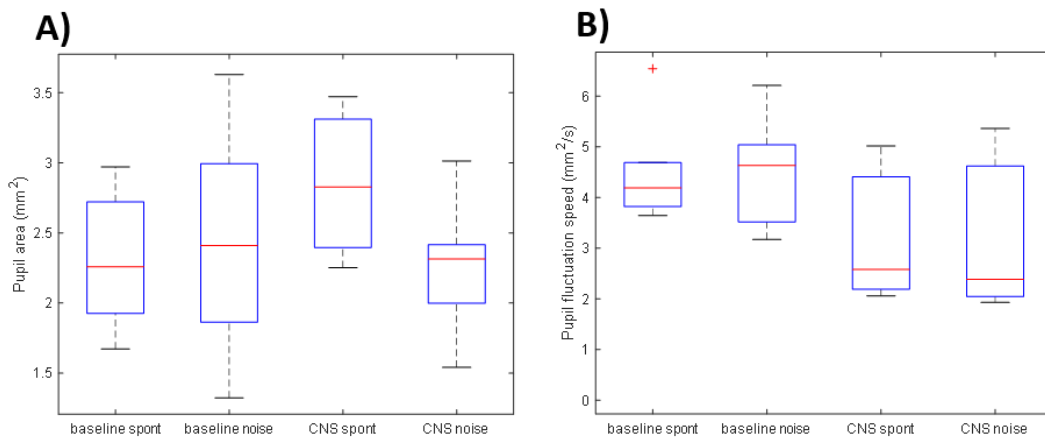


**Figure 15. Pupil activity for CNS animals during recordings.** A) Pupil area (mm<sup>2</sup>) for CNS animals in all recording conditions. Red line indicates mean value. B) Pupil fluctuation speed (mm<sup>2</sup>/s) for CNS animals in all recording conditions.

### 2.4.2. Brain morphology

Mean brain volume was calculated for stress and control groups from 3.2mm from bregma to -6.8mm from bregma (Figure 16). A two sample t-test for the average brain volume revealed significant brain shrinkage in the CNS group compared with controls ( $t(8) = 4.941, p = 0.001$ ).

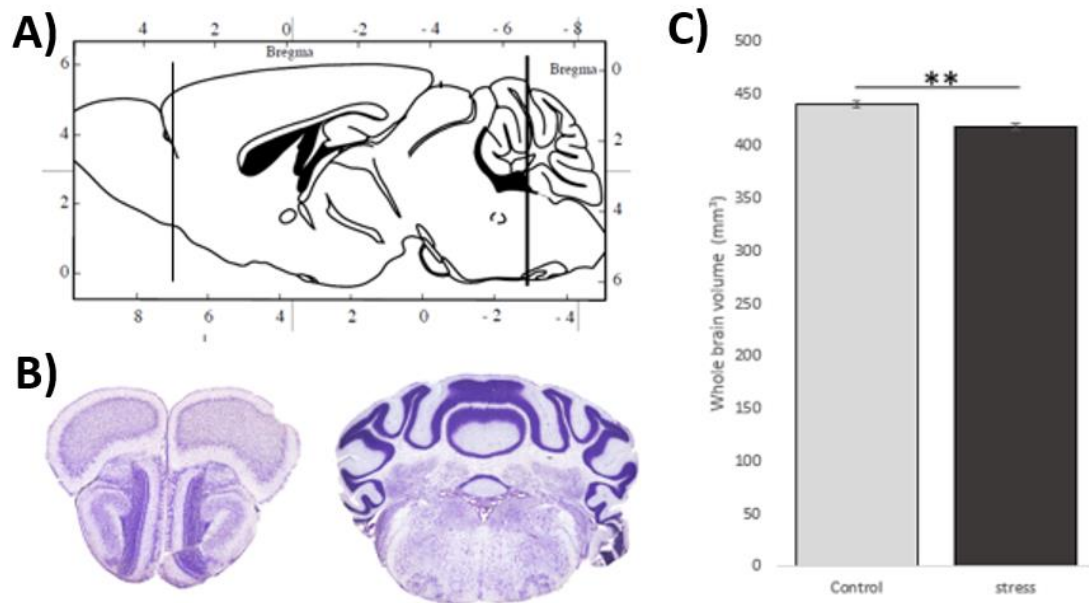


**Figure 16: Mean brain volumes of stress and control animals.** A) Schematic of area of the brain from which samples were collected for volumetric analysis. B) Example of first and last cresyl violet-stained sections collected for analysis. C) Volumetric difference (mm<sup>3</sup>) between all stress and control animal brains. Results presented as mean  $\pm$  S.E.M. Asterisk indicates  $*p < 0.0025$ .

Mean amygdala volume was calculated for the basolateral nucleus in stress and control animals (Figure 17). A two-sample t-test for the average amygdala volume revealed no significant difference between stress and control groups ( $t(8) = 0.346, p = 0.738$ ).

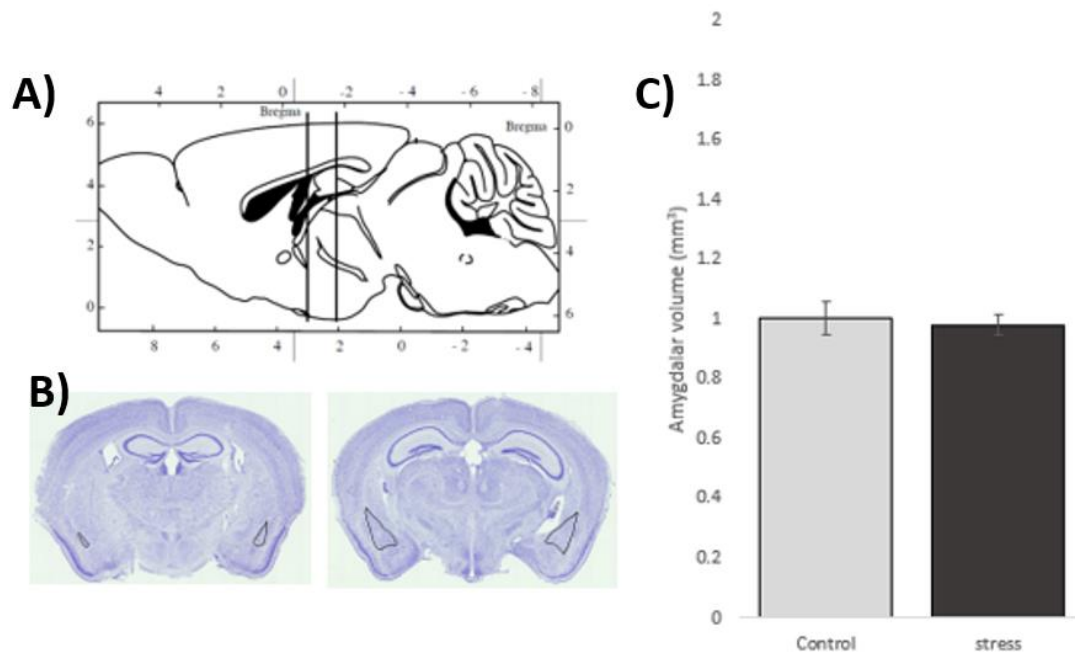


**Figure 17: Mean amygdala volumes of stress and control animals.** A) Schematic of area of the brain from which samples were collected for volumetric analysis. B) Example of first and last cresyl violet-stained sections collected for analysis. C) Volumetric difference (mm<sup>3</sup>) for all stress and control animals. Results presented as mean  $\pm$  S.E.M.

Average hippocampal volume was calculated for each group, and a two-sample t-test revealed significant shrinkage in the CNS group compared with controls ( $t(8) = 4.614$ ,  $p = 0.02$ ) (Figure 18).

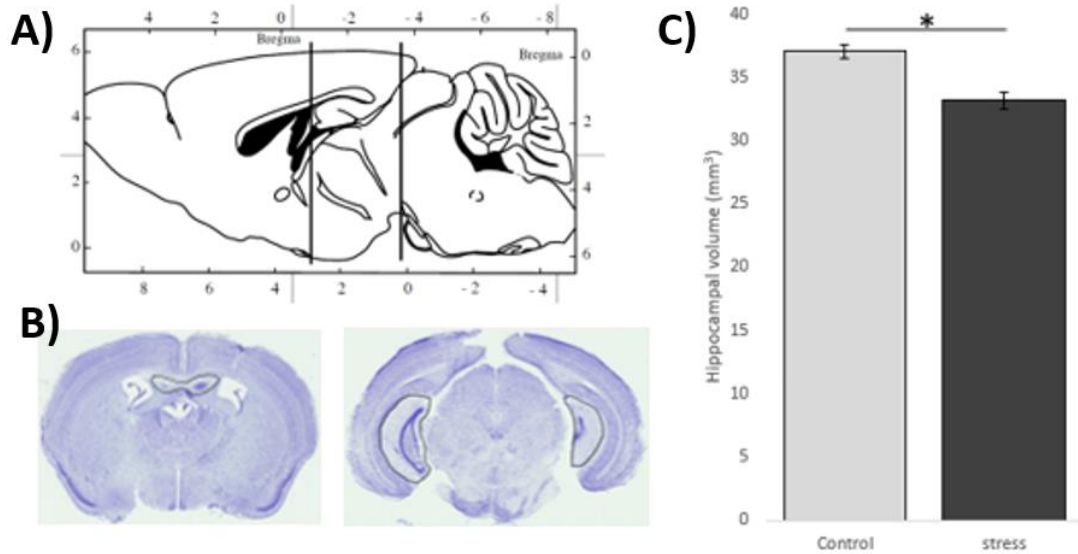


**Figure 18: Mean hippocampal volumes of stress and control animals.** A) Schematic of area of the brain from which samples were collected for volumetric analysis. B) Example of first and last cresyl violet-stained sections collected for analysis. C) Volumetric difference (mm<sup>3</sup>) between all stress and control animal brains. Results presented as mean  $\pm$  S.E.M. Asterisk indicates  $*p < 0.05$ .

Cortical thickness was reduced in the CNS compared with controls in all ventral, lateral, and ventrolateral measurements (Figures 19-25). A two sample t-test for each measure

revealed significance of the ventral measurement 2.46 mm from bregma

( $t(8) = 2.4870.782$ ,  $p = 0.038$ ), -2.22 mm ( $t(8) = 2.688$ ,  $p = 0.028$ ), 1.42 mm ( $t(8) = 3.816$ ,

$p = 0.005$ ), -1.10 mm ( $t(8) = 2.265$ ,  $p = 0.01$ ), and 0.50 mm ( $t(8) = 3.326$ ,  $p = 0.01$ ) from

bregma. The lateral measurement was significant at 2.22 mm ( $t(8) = 9.025$ ,  $p = 0.001$ )

and 1.42 mm ( $t(8) = 2.861$ ,  $p = 0.021$ ) from bregma. The ventrolateral measurement was

significant at 2.46 mm ( $t(8) = 3.755$ ,  $p = 0.006$ ) and 2.22 mm ( $t(8) = 6.258$ ,  $p = 0.001$ )

from bregma.

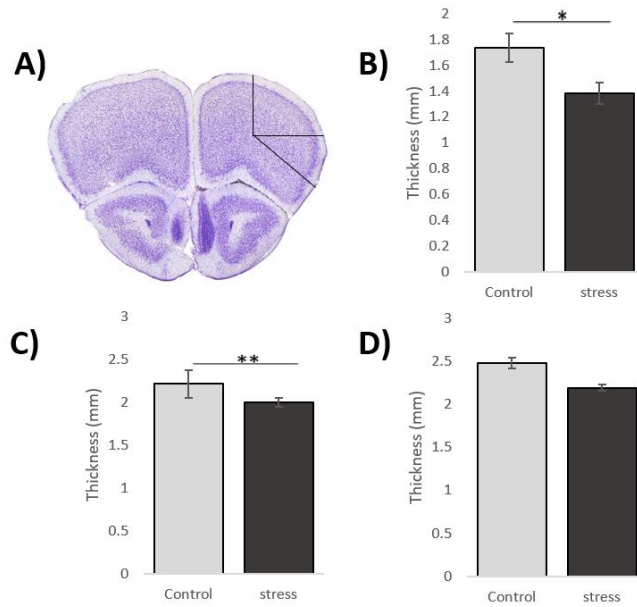


**Figure 19. Cortical thickness measures 2.46 mm from bregma.** A) Nissl-stained brain section 2.46mm from bregma showing the lines along which measurements were taken. B) Central cortical thickness for CNS and controls. C) Lateral cortical thickness for CNS and controls. D) Ventrolateral cortical thickness for CNS and controls. Results presented as mean  $\pm$  S.E.M. Asterisks indicate  $*p < 0.05$  or  $**p < 0.025$ .

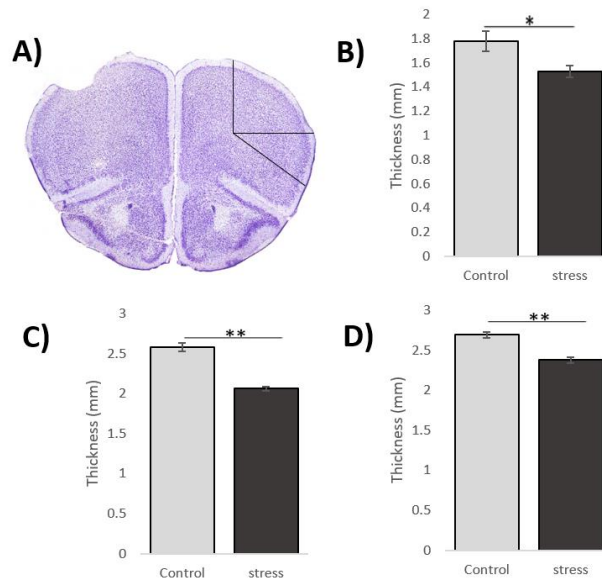


**Figure 20. Cortical thickness measures 2.22 mm from bregma.** A) Nissl-stained brain section 2.22 mm from bregma showing the lines along which measurements were taken. B) Central cortical thickness for CNS and controls. C) Lateral cortical thickness for CNS and controls. D) Ventrolateral cortical thickness for CNS and controls. Results presented as mean  $\pm$  S.E.M. Asterisks indicate  $*p < 0.05$  or  $**p < 0.025$ .

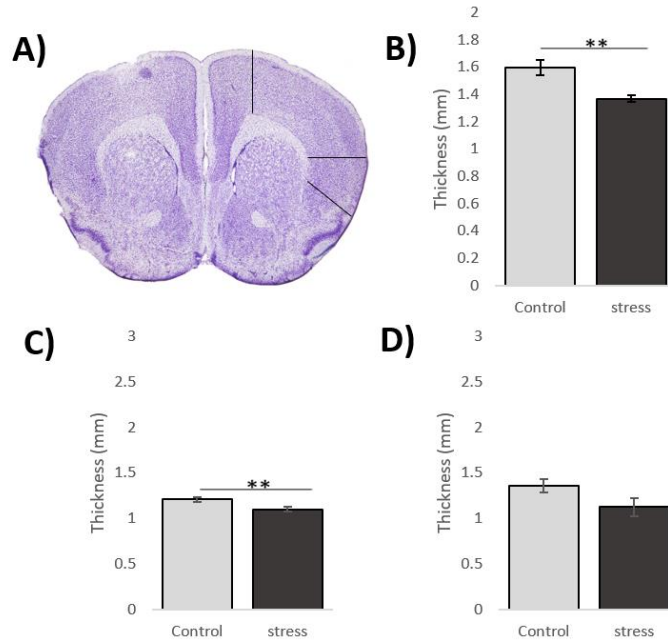


**Figure 21. Cortical thickness measures 1.42 mm from bregma.** A) Nissl-stained brain section 1.42 mm from bregma showing the lines along which measurements were taken. B) Central cortical thickness for CNS and controls. C) Lateral cortical thickness for CNS and controls. D) Ventrolateral cortical thickness for CNS and controls. Results presented as mean  $\pm$  S.E.M. Asterisks indicate  $**p < 0.025$ .

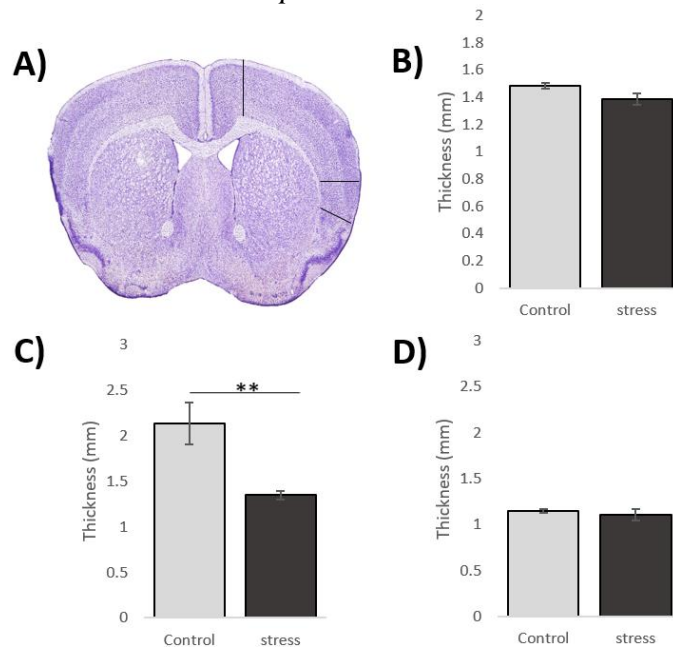


**Figure 22. Cortical thickness measures 1.10 mm from bregma.** A) Nissl-stained brain section 1.10 mm from bregma showing the lines along which measurements were taken. B) Central cortical thickness for CNS and controls. C) Lateral cortical thickness for CNS and controls. D) Ventrolateral cortical thickness for CNS and controls. Results presented as mean  $\pm$  S.E.M. Asterisks indicate  $**p < 0.025$ .

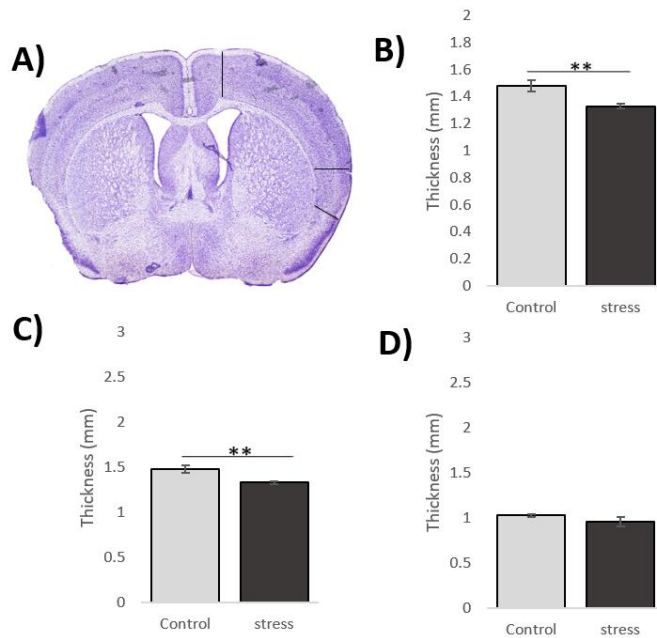


**Figure 23. Cortical thickness measures 0.50 mm from bregma.** A) Nissl-stained brain section 0.50 mm from bregma showing the lines along which measurements were taken. B) Central cortical thickness for CNS and controls. C) Lateral cortical thickness for CNS and controls. D) Ventrolateral cortical thickness for CNS and controls. Results presented as mean  $\pm$  S.E.M. Asterisks indicate  $**p < 0.025$ .

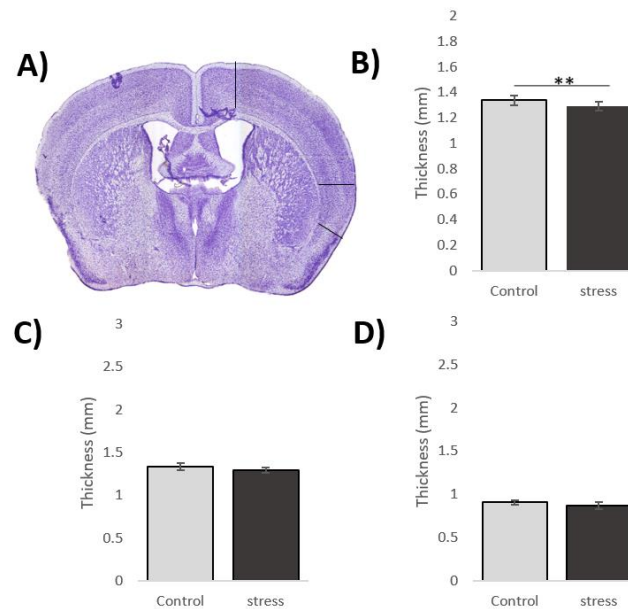


**Figure 24. Cortical thickness measures -0.10 mm from bregma.** A) Nissl-stained brain section -0.10 mm from bregma showing the lines along which measurements were taken. B) Central cortical thickness for CNS and controls. C) Lateral cortical thickness for CNS and controls. D) Ventrolateral cortical thickness for CNS and controls. Results presented as mean  $\pm$  S.E.M. Asterisks indicate  $**p < 0.025$ .

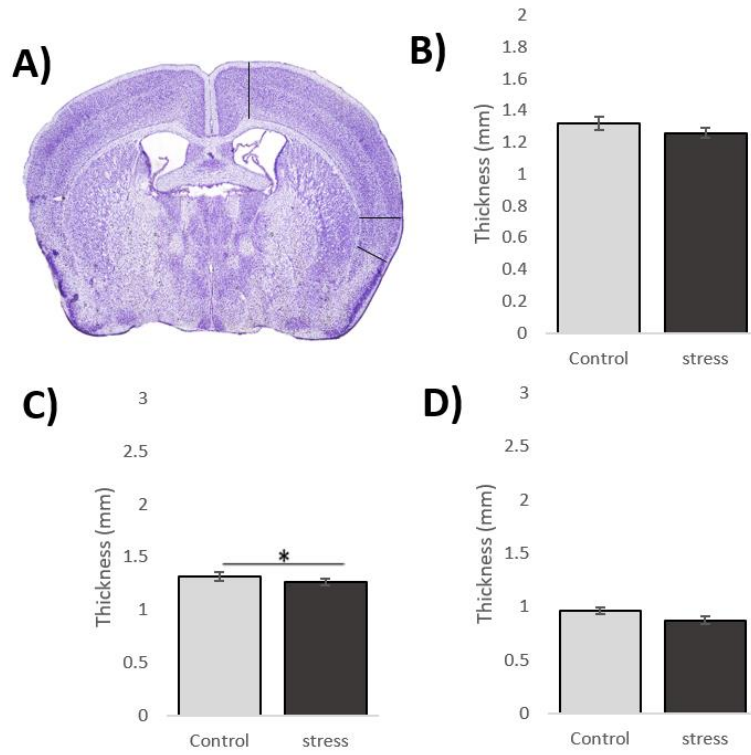


**Figure 25. Cortical thickness measures -0.70 mm from bregma.** A) Nissl-stained brain section -0.70 mm from bregma showing the lines along which measurements were taken. B) Central cortical thickness for CNS and controls. C) Lateral cortical thickness for CNS and controls. D) Ventrolateral cortical thickness for CNS and controls. Results presented as mean  $\pm$  S.E.M. Asterisks indicate  $*p < 0.05$ .

### 2.4.3. Cortical connectivity

Cortical correlations were computed for 18 ROIs for a total of 153 possible ROI combinations to measure intracortical connectivity and compared between all recording conditions in CNS and control animals. A two-sample t-test for each ROI combination revealed no significant differences in average correlation ( $p \geq 0.05$ ) between the spontaneous and noise conditions in control animals (Figure 26 – C, F). There was also no significant difference between the baseline spontaneous and spontaneous recordings after 30 days in the control condition (Figure 26 – G). There was a significant increase in correlation between HLS2B vs. FLS2 ( $t(16) = 2.3333, p = 0.0330$ ) and mFL vs. mHL ( $t(16) = 2.2983, p = 0.0354$ ), and a significant decrease in correlation between Aud vs. FLS2 ( $t(16) = -2.2637, p = 0.0378$ ) between the baseline noise recordings and the noise recordings after 30 days in the control condition (Figure 26 – H).

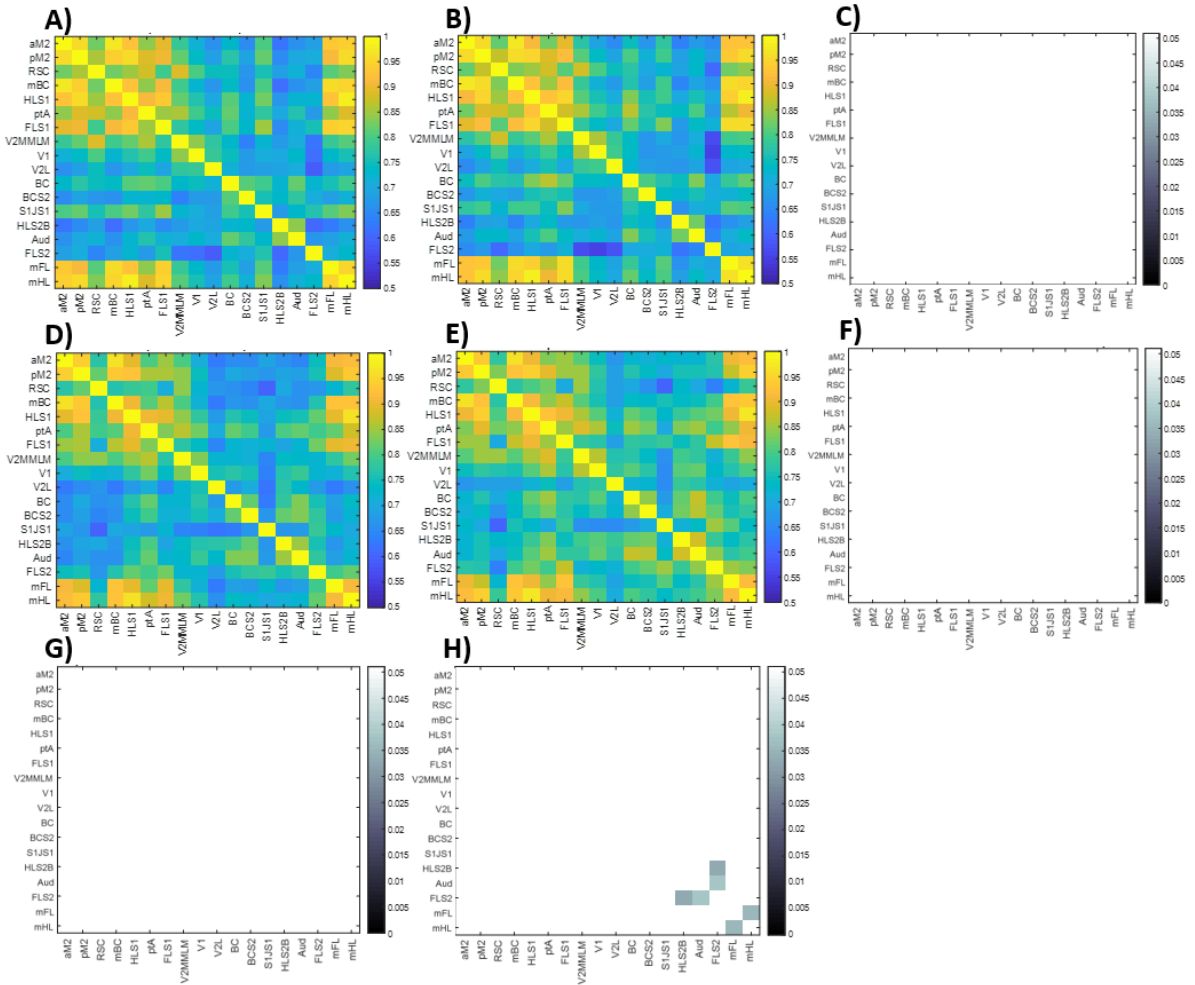


**Figure 26. Cortical correlations for control animals.** A) Correlation matrix for baseline spontaneous activity. B) Correlation matrix for baseline activity with noise played in the recording chamber. C) Significance values for correlation between baseline spontaneous and baseline noise condition activity. White regions are not significant ( $p \geq 0.05$ ). D) Cortical correlation matrix for spontaneous activity after 30 days in the control condition. E) Correlation matrix for activity with noise played in the recording chamber after 30 days in the control condition. F) Significance values for correlation between spontaneous and noise condition activity after 30 days in the control condition. White regions are not significant ( $p \geq 0.05$ ). G) Significance values for correlation between the baseline spontaneous activity and the spontaneous activity after 30 days in the control condition. White regions are not significant ( $p \geq 0.05$ ). H) Significance values for correlation between the baseline activity in the noise condition and activity in the noise condition after 30 days in the control condition. White regions are not significant, non-white regions are significant ( $p < 0.05$ ).

The overall average correlation was computed for all control animals (Figure 27). The average baseline spontaneous recordings in control animals was 0.7559, which decreased slightly to 0.7347 in the baseline noise recording. The overall average correlation for spontaneous activity after 30 days in the control condition increased from the baseline value to 0.7733, which increased slightly in the noise recording after 30 days in the control condition to 0.8033. A two-sample t-test revealed no significant difference in overall average correlation between any recording condition for control animals ( $p \geq 0.05$ ).

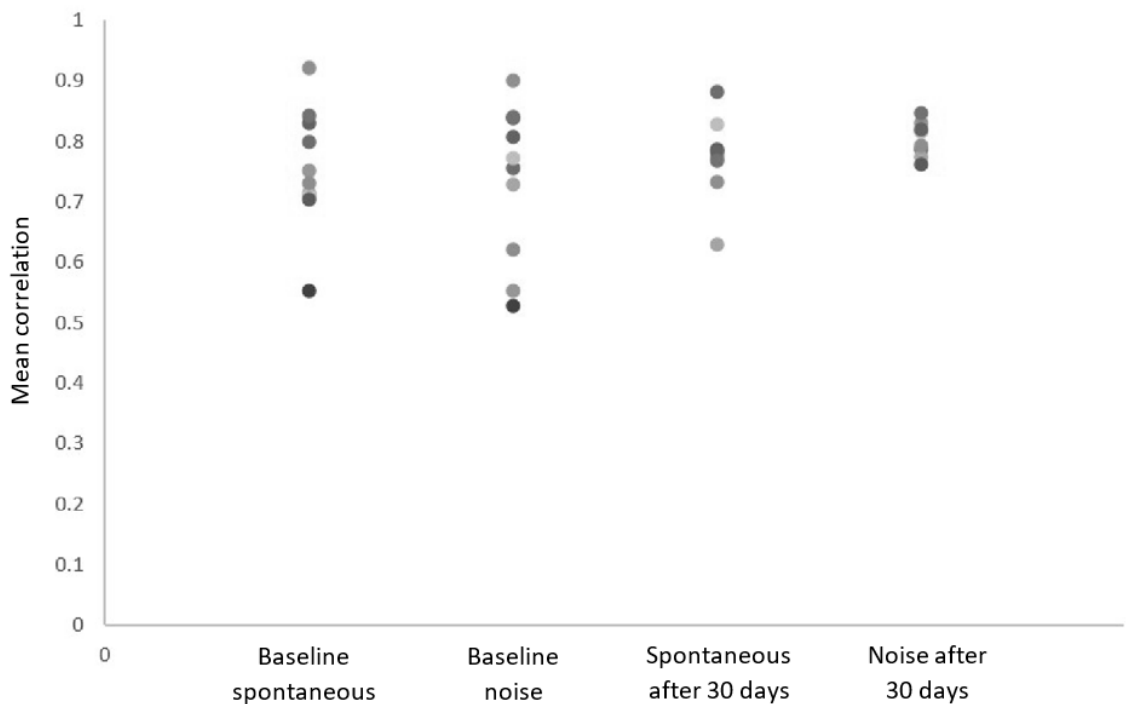


**Figure 27. Average cortical correlation for control animals.** Overall mean correlation values for each recording condition in each control animal.

A two-sample t-test of each ROI combination revealed no significant difference in average correlation between the baseline spontaneous and noise recording conditions for CNS animals ( $p \geq 0.05$ ) (Figure 28 – C). There was a significant increase in correlation between FLS1 vs. BC ( $t(16) = 2.1900, p = 0.0437$ ), FLS1 vs. S1JS1 ( $t(16) = 2.2175, p = 0.0414$ ), BC vs. mFL ( $t(16) = 2.4129, p = 0.0282$ ), and S1JS1 vs. mFL ( $t(16) = 2.1831, p = 0.0443$ ) between the spontaneous and noise recordings after 30 days CNS (Figure 28 – F). Significant changes were found between the baseline spontaneous and spontaneous after 30 days CNS conditions for 13 ROI combinations (Figure 28 – G, table 1). Significant differences in average correlation were also found in 8 ROI combinations between the baseline noise and noise after 30 days CNS conditions (Figure 28 – H, table 2).

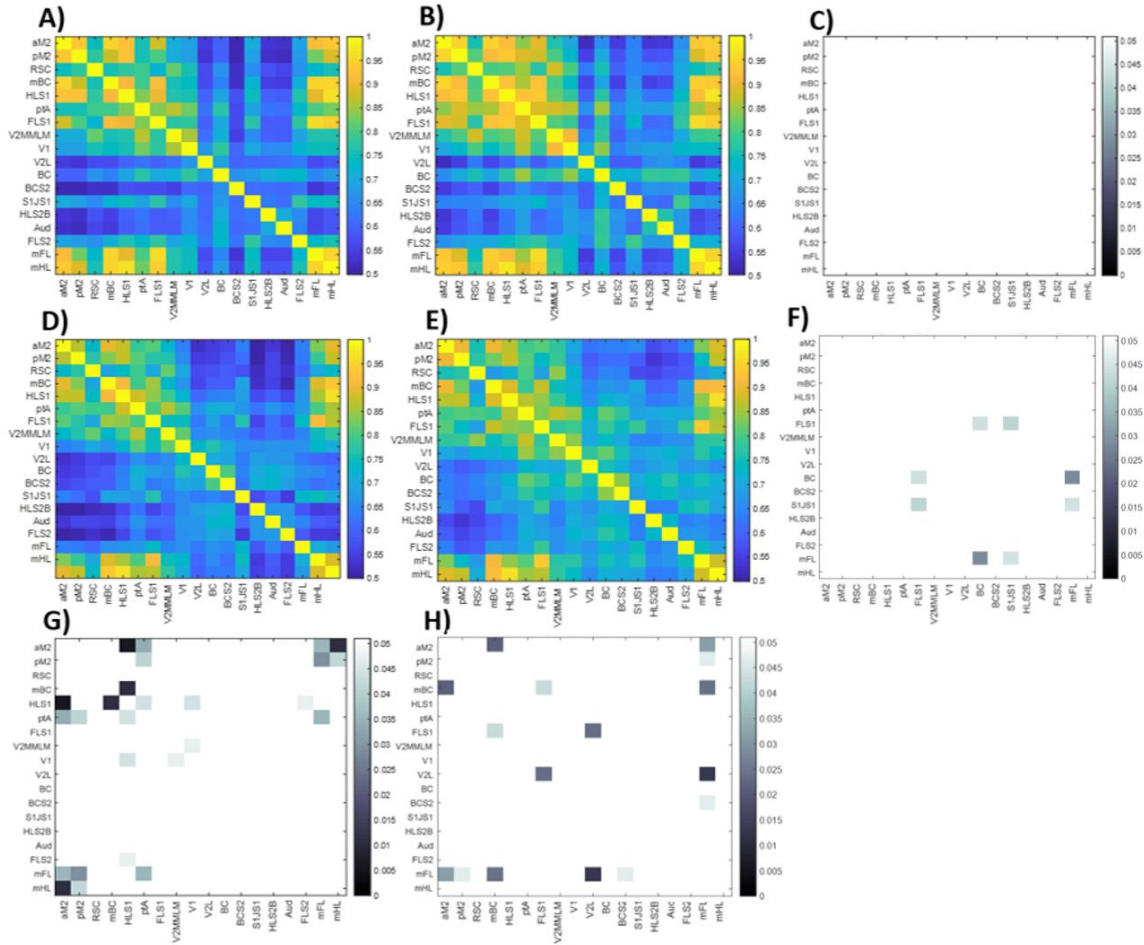


**Figure 28. Cortical correlations for stress animals.** A) Correlation matrix for baseline spontaneous activity. B) Correlation matrix for baseline activity with noise played in the recording chamber. C) Significance values for correlation between baseline spontaneous and baseline noise condition activity. White regions are not significant ( $p \geq 0.05$ ). D) Cortical correlation matrix for spontaneous activity after 30 days in the stress condition. E) Correlation matrix for activity with noise played in the recording chamber after 30 days in the stress condition. F) Significance values for correlation between spontaneous and noise condition activity after 30 days in the stress condition. White regions are not significant, non-white regions are significant ( $p < 0.05$ ). G) Significance values for correlation between the baseline spontaneous activity and the spontaneous activity after 30 days in the stress condition. White regions are not significant, non-white regions are significant ( $p < 0.05$ ). H) Significance values for correlation between the baseline activity in the noise condition and activity in the noise condition after 30 days in the stress condition. White regions are not significant, non-white regions are significant ( $p < 0.05$ ).

**Table 1: Statistical values for CNS animals between spontaneous recordings.**

<b>Regions</b>	<b><i>t</i>(13)-value</b>	<b><i>p</i>-value</b>
aM2 vs. mHL	-3.2500	0.0063
aM2 vs. mFL	-2.3689	0.0340
aM2 vs. ptA	-2.3506	0.0352
aM2 vs. HLS1	-2.9570	0.0111
pM2 vs. mHL	-2.2696	0.0410
pM2 vs. mFL	-2.4505	0.0292
pM2 vs. ptA	-2.2620	0.0415
mBC vs. HLS1	-2.9708	0.0108
HLS1 vs. FLS2	-2.2224	0.0446
HLS1 vs. V1	-2.2272	0.0442
HLS1 vs. ptA	-2.2100	0.0473
ptA vs. mFL	-2.3415	0.0358
V2MMLM vs. V1	-2.1879	0.0475

**Table 2. Statistical values for CNS animals between noise recordings.**

<b>Regions</b>	<b><i>t</i>(14)-value</b>	<b><i>p</i>-value</b>
aM2 vs. mBC	-2.6002	0.0210
aM2 vs. mFL	-2.3954	0.0311
pM2 vs. mFL	-2.1791	0.0469
mBC vs. FLS1	-2.2295	0.0427
mBC vs. mFL	-2.5297	0.0240
FLS1 vs. V2L	2.5388	0.0236
V2L vs. mFL	2.8484	0.0129
BCS2 vs. mFL	2.1825	0.0466

The overall average correlation was computed for all stress animals (Figure 29). The overall average correlation for baseline spontaneous recordings of CNS animals was 0.7341, which decreased insignificantly ( $p \geq 0.05$ ) in the baseline noise recording to 0.7260. The overall average correlation for spontaneous recordings after 30 days CNS decreased from the baseline value to 0.6872. The overall average correlation for noise recordings after 30 days CNS was 0.7359, a slight increase from the baseline value and an

increase from the post-CNS spontaneous value. None of the changes in overall correlation between any recording conditions were significant ( $p \geq 0.05$ ).

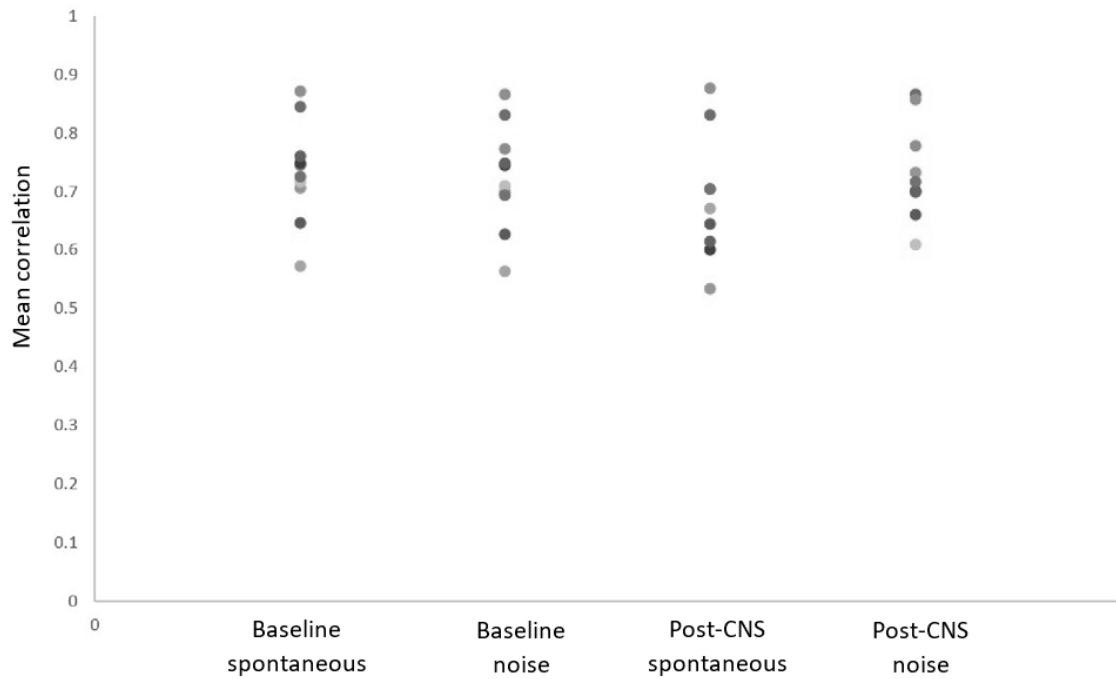


**Figure 29. Average cortical correlation for stress animals.** Overall mean correlation values for each recording condition in each CNS animal.

#### 2.4.4. Electrophysiology

The probability of the vHPC or BLA leading synchrony for each peak of theta activity was computed for CNS and control animals. Significance was defined at  $p = 0.025$  based on a Bonferroni correction for each comparison. A two-sample t-test showed no significant difference in mean values between the baseline spontaneous and baseline noise conditions for control animals ( $t(6) = -1.383, p = 0.216$ ) (Figure 30 – A, B). There was also no significant difference in theta synchrony between the spontaneous baseline and spontaneous recording after 30 days in the control environment ( $t(6) = -1.296, p = 0.243$ ) (Figure 30 – A, C), between the noise baseline and noise recording after 30 days in the control environment ( $t(8) = -1.674, p = 0.133$ ) (Figure 30 – B, D), or between the spontaneous and noise conditions after 30 days in the control environment ( $t(8) = -1.617, p = 0.145$ ) (Figure 30 – C, D).

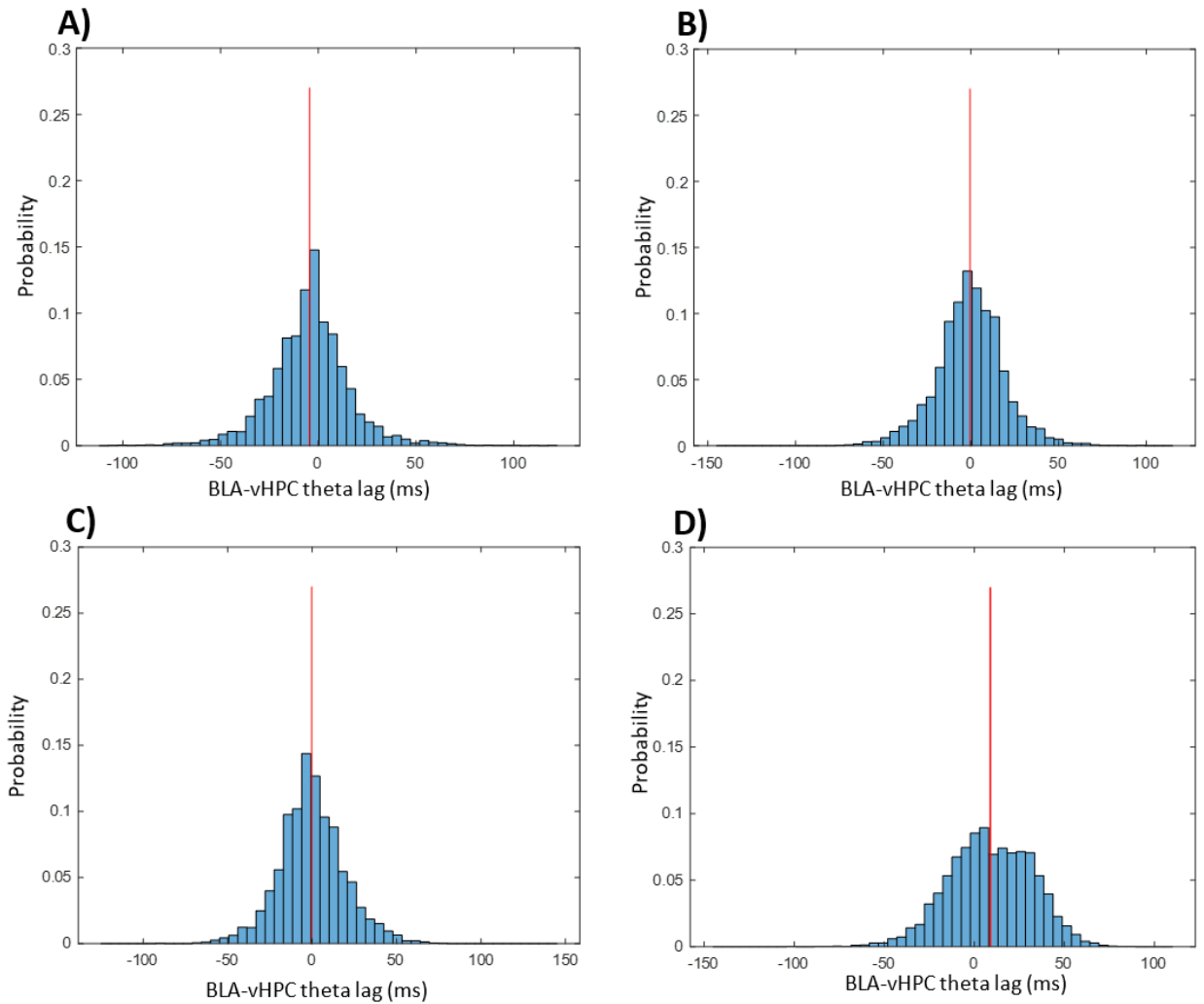


**Figure 30. Leading/lagging theta activity in BLA and vHPC of control animals.**

A) Histogram depicting the probability distribution of vHPC or BLA leading theta activity synchrony in the baseline spontaneous recording condition. Positive x-axis values indicate the BLA leading, negative values indicate the vHPC leads. The red line represents the mean (-5 ms). B) Histogram depicting the probability distribution of vHPC or BLA leading theta activity synchrony in the baseline noise recording condition. Positive x-axis values indicate the BLA leading, negative values indicate the vHPC leads. Mean lead/lag time = 0.3 ms (red line). C) Histogram depicting the probability distribution of vHPC or BLA leading theta activity synchrony in the spontaneous recording condition after 30 days in the control condition. Positive x-axis values indicate the BLA leading, negative values indicate the vHPC leads. Mean lead/lag time = - 0.1 ms (red line). D) Histogram depicting the probability distribution of vHPC or BLA leading theta activity synchrony in the noise recording condition after 30 days in the control condition. Positive x-axis values indicate the BLA leading, negative values indicate the vHPC leads. Mean lead/lag time = 7 ms (red line).

A two-sample t-test revealed no significant change between mean theta synchrony from the baseline spontaneous to the noise recording conditions for CNS animals ( $t(5) = 1.355$ ,  $p = 0.233$ ) (Figure 31 – A, B). There was a significant shift towards BLA-leading theta synchrony between the baseline spontaneous recordings and the spontaneous recordings after 30 days CNS ( $t(5) = -3.311$ ,  $p = 0.021$ ) (Figure 31 – A, C), but no significant difference between the baseline noise recording and the noise recording after 30 days CNS ( $t(6) = -0.746$ ,  $p = 0.484$ ) (Figure 31 – B, D). There was also no significant change between the spontaneous and noise recording conditions after 30 days CNS ( $t(6) = 1.772$ ,  $p = 0.127$ ) (Figure 31 – C, D).

There was no significant difference between the baseline recordings in control or CNS animals in the spontaneous condition ( $t(4) = -0.456$ ,  $p = 0.672$ ) (Figure 30 – A, Figure 31 – A), or in the noise condition ( $t(7) = 0.958$ ,  $p = 0.370$ ) (Figure 30 – B, Figure 31 – B). There was a significant shift towards BLA-leading theta synchrony in spontaneous recordings for animals exposed to 30 days CNS compared with animals that spent 30 days in the control environment ( $t(7) = -3.672$ ,  $p = 0.008$ ) (Figure 30 – C, figure 31 – C). No significant difference was found between the CNS and controls in the noise recording condition after 30 days ( $t(7) = 0.653$ ,  $p = 0.535$ ) (Figure 30 – D, Figure 31 – D).

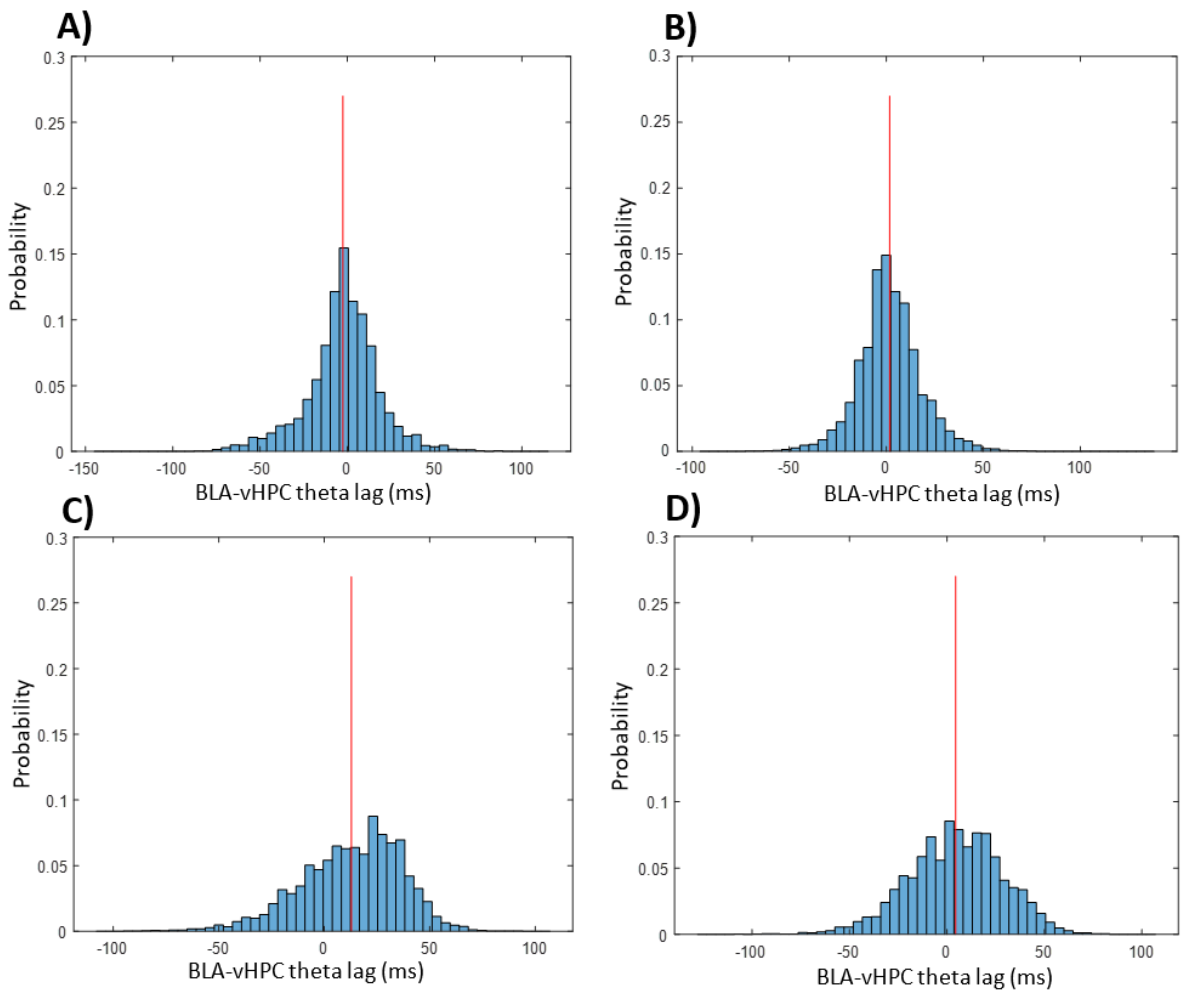


**Figure 31. Leading/lagging theta activity in BLA and vHPC of CNS animals.** A) Histogram depicting the probability distribution of vHPC or BLA leading theta activity synchrony in the baseline spontaneous recording condition. Positive x-axis values indicate the BLA leading, negative values indicate the vHPC leads. The red line represents the mean (-4 ms). B) Histogram depicting the probability distribution of vHPC or BLA leading theta activity synchrony in the baseline noise recording condition. Positive x-axis values indicate the BLA leading, negative values indicate the vHPC leads. Mean lead/lag time = 2 ms (red line). C) Histogram depicting the probability distribution of vHPC or BLA leading theta activity synchrony in the spontaneous recording condition after 30 days of CNS. Positive x-axis values indicate the BLA leading, negative values indicate the vHPC leads. Mean lead/lag time = 15 ms (red line). D) Histogram depicting the probability distribution of vHPC or BLA leading theta activity synchrony in the noise recording condition after 30 days of CNS. Positive x-axis values indicate the BLA leading, negative values indicate the vHPC leads. Mean lead/lag time = 5 ms (red line).

### 3. Discussion

This thesis aimed to identify the brain and behavioural correlates of chronic noise stress in a network between the vHPC, BLA, and a unilateral section of the neocortex. To achieve this aim, widefield Glu imaging of spontaneous cortical activity and LFP activity in the BLA and vHPC were recorded in quiet conditions and noisy conditions for mice exposed to chronic noise and unstressed controls. These recordings quantified significant changes between CNS and control groups after the 30-day stress intervention. Pupil activity data was also collected to determine a behavioural correlate of each recording condition. A change in pupil area and speed of fluctuation was observed between stress and control groups and within spontaneous and noise recording conditions, but these changes were not statistically significant. As shown previously, (Jafari, Kolb et al. 2018, Jafari, Kolb et al. 2020) Cresyl violet histology revealed the morphological correlates of network-level changes, including significant shrinkage of the hippocampus, decreased cortical thickness, and overall brain shrinkage in the CNS animals.

The small  $N$ -value used for statistical analysis was due to surgical complications related to excessive ageing and degradation of windows and electrodes over time in some animals. Males ( $N = 6$ ; 3 per group) and females ( $N = 4$ ; 2 per group) were pooled for analysis, which may have affected the statistical outcome of the observed stress effects. This method of pooling males and females for statistical analysis also was used by Jafari et al. (2018) when a multi-way ANOVA revealed no statistical significance in brain morphology between sex and chronic noise stress or control conditions. However, some chronic stress studies have demonstrated dimorphic neural and behavioural symptoms in rodent and human males and females (Brivio, Lopez et al. 2020), and imaging studies in

rats have shown that females may be more vulnerable to chronic-stress induced behavioural and network level effects (Lin, Ter Horst et al. 2009). Histological findings may also have been affected by combining males and females for statistical analysis, which will be discussed in section 3.2. Repeating these experiments with  $N = 20$ , the number of subjects originally planned, would provide the statistical power needed to draw reliable conclusions on the effects of sex, group (chronic noise stress or control), and recording condition (spontaneous or noise) on brain networks and behaviour. However, males and females do appear to exhibit some similar neural and behavioural symptoms beyond some threshold of chronic stress exposure (Lin, Ter Horst et al. 2009, Jafari, Kolb et al. 2018), suggesting that the significant effects observed in this thesis are useful as broad foundations for understanding behavioural and network-level changes due to CNS.

### **3.1. Chronic and acute noise exposure alters pupil activity**

Mammalian pupils fluctuate in response to changes in environmental luminance via connections with the pretectal nuclei, and in response to changes in attention or arousal due to changes in cortical state (Reimer, McGinley et al. 2016). When light conditions are controlled for, pupil activity can be used as a reliable measure of affective state in response to a punctate stimulus (Ehlers, Strauch et al. 2016, Henderson, Bradley et al. 2018, Schriver, Bagdasarov et al. 2018). However, less is known about how the pupil reacts to prolonged affective stimuli, such as 15 mins acute traffic noise exposure.

Concurrent recordings of pupil dilation, heart rate, and skin conductance consistently report that pupil dilation correlates to sympathetic nervous system activity (Yamanaka and Kawakami 2009, Henderson, Bradley et al. 2018). Pupil fluctuation studies using affective imagery to elicit the nonspecific stress response show that pupil diameter is

larger in response to stressful stimuli, that these stimuli increase the time the pupil remains dilated, and that heightened pupil reactivity to stressful stimuli may predict depressive symptoms (Bradley 2017, Feurer, Burkhouse et al. 2017). These could be the effects of noise exposure observed in this thesis, with increased average pupil size and decreased fluctuation speed in CNS animals corresponding to increased SAM- and HPA-axis activity.

Pupil activity has also been studied in the presence of acute auditory stressors in fear learning experiments, and fluctuation is thought to measure psychological stress in anticipation of an aversive stimulus. Fear learning also activates and alters BLA-vHPC network activity, and a heightened fear response due to chronic stress has been implicated as contributing to anxiety, depression, and PTSD (Britton, Lissek et al. 2011, Moustafa, Gilbertson et al. 2013, Maren and Holmes 2016). These studies consistently report distinct pupil dilation in response to an aversive conditioned auditory stimulus (Korn, Staib et al. 2017, Leuchs, Schneider et al. 2017), which demonstrates the utility of pupil fluctuation as a measure of psychological stress in response to an auditory stimulus independent of visual system activation.

Pupil fluctuations were analyzed in this thesis as a convenient and non-invasive behavioural measure of affective state that could be recorded in head-fixed mice.

Although there was no significant change in average pupil area or average fluctuation speed between any recording condition, there was more variability in pupil area during the noise recording conditions in CNS and control animals, and a decrease in average pupil fluctuation speed after 30 days noise stress in the CNS animals that was not found in controls. These findings may support the hypothesis that noise exposure elicits a

behavioural stress response, but they may also indicate that pupil fluctuations were not an optimal measure of affective state throughout the duration of a 15 min head-fixed recording. A larger number of experimental animals and alternative non-invasive behavioural measures (e.g. body weight and home cage behavioural monitoring, (Singh, Bermudez-Contreras et al. 2019)) would be needed to determine whether concurrent pupil changes support the conclusion that CNS can provoke behavioural symptoms reflected in pupil activity.

Pupil fluctuation and its concurrent activation with the SAM system in response to affective stimuli have also been linked to global neural activity and the activity of cell populations (Lee and Margolis 2016, Reimer, McGinley et al. 2016). Further research and analysis correlating pupil fluctuation in response to a punctate stressor with concurrent recordings of neural activity could provide a non-invasive behavioural measure of chronic stress-induced cortical changes.

### **3.2. Chronic noise stress creates changes in brain morphology**

Significant reductions in hippocampal volume, cortical thickness, and overall brain volume were found in mice exposed to chronic noise stress, as shown previously (Jafari, Kolb et al. 2018). Although stressed mice also showed a small reduction in amygdala volume, these changes were not statistically significant. The findings in this thesis support the hypothesis that chronic noise exposure induces the structural changes to brain morphology that are characteristic of chronic stress and its psychological symptoms. However, issues of small sample size, the methods used to evaluate brain size, and the methods of analysis in this thesis may confound these findings and prevent a reliable conclusion.

Combining males and females for statistical analysis could have affected the results of this thesis, as sex differences in average brain volume have been established in humans and mice. One study of neural morphology in mice with a larger sample size ( $N = 8$  males and 8 females per group) found no significant difference in CNS-induced changes in brain volume of male and female animals (Jafari, Kolb et al. 2018), however, MRI studies in humans have shown that stress can have unique morphological effects in females and males (McLaughlin, Baran et al. 2009). A larger sample size with statistics performed on males and females separately would be needed to reliably conclude that CNS triggers HPC and cortical atrophy in males and females using the chronic noise methods in this thesis.

This study of neural morphology in mice also used perfused and cresyl violet-stained brain sections, which require precision to ensure that perfusion, storage, and sectioning of brain tissue are consistent because each intervention can affect volumetric estimates. A more reliable measure of brain size could be the weight of brains without perfusion. This method has its own issues, however, as the soft brain tissue is easier to damage during extraction and the volume of particular structures cannot be estimated. Histological analysis also allows for measures of cell density within neural regions, which would demonstrate whether stress-induced changes are due to neural atrophy or hypertrophy. A large sample size, precise perfusions and storage of brain tissue, and further analysis of cell density would be needed to determine whether chronic noise reliably induces the hippocampal and cortical atrophy quantified in this thesis.

Alterations to hippocampal morphology match findings in rodent models of stress and magnetic resonance imaging (MRI) studies which quantify structural changes in

chronically stressed and subjects. Chronic stress is known to cause hippocampal atrophy in rodents (Lee, Jarome et al. 2009). A loss of hippocampal volume has also been documented in individuals suffering from major depressive disorder (MDD) and PTSD, and effective treatments for these disorders have been shown to increase hippocampal volume (Gianaros, Jennings et al. 2007, Sheline, Liston et al. 2019). These structural changes have been shown to involve a loss of pyramidal cell density and complexity, and an overall decrease in HPC volume due to stress-induced atrophy (Jafari, Kolb et al. 2018, Patel, Kas et al. 2019). Chronic stress has also been shown to induce a loss of dendritic spines and fewer and smaller cells in the CA1 region of the vHPC (Pawlak, Rao et al. 2005), which may induce changes in intraregional activity and extraregional connections.

Cell atrophy in response to chronic stress may be mediated by neurotrophic factors, which are neuromodulatory molecules that can induce structural changes in the brain (Patel, Kas et al. 2019). Brain-derived neurotrophic factor (BDNF) and its receptor, tyrosine kinase receptor B, have been established as mediators of neuroplasticity and are essential for neuronal health. Chronic stress has been shown to damage cells producing BDNF in the hippocampus via excess circulating CORT, which may cause stress-induced hippocampal atrophy (Pawlak, Rao et al. 2005, Pittenger and Duman 2008, Patel, Kas et al. 2019).

Stress-induced reductions in cortical thickness and brain volume have also been documented in response to chronic noise stress (Jafari, Kolb et al. 2018). This atrophy may be due to a reduced number of astrocytes in the brain, which reduces the brain's ability to clear excess extracellular Glu from the synaptic clefts. This excess and prolonged exposure to Glu has been shown to have excitotoxic effects by destroying

NMDARs and AMPARs, leading to behavioural and psychological symptoms (Patel, Kas et al. 2019). Astrocytes are also responsible for the synthesis and release of BDNF, and their damage may be responsible for changes to HPC and BLA morphology reported in chronic stress experiments (Patel, Kas et al. 2019).

No significant effects of chronic noise stress on amygdala volume were observed in this thesis, and published literature provides inconsistent results for the effects of chronic stress on amygdala morphology. Some studies have found increased BDNF levels leading to dendritic hypertrophy and an increase in amygdala volume (Lange and Irle 2004, Hamilton, Siemer et al. 2008), whereas others report a decrease in amygdala volume in response to chronic CORT exposure (Brown, Woolston et al. 2008). These conflicting findings could be due to the different modes and durations of stress used. It has been suggested that amygdala hypertrophy may be due to stressful thought rumination, which activates and strengthens stress network activity over time. However, a chemical stressor such as CORT treatment could produce the atrophic effects via similar excitotoxic mechanisms thought to cause hippocampal atrophy due to chronic stress. The duration of exposure to a chronic stressor is also relevant to hippocampal and amygdala functioning and morphological changes. The effects of Glu on HPC MRs are rapid and reversible but produce slower and longer lasting effects in the BLA (Hermans, Battaglia et al. 2014). It is possible that the excitotoxic effects of damaged and destroyed MRs in the BLA requires a longer duration of chronic stress exposure to elicit the effects observed in the HPC after only 30 days of CNS.

### **3.3. Chronic noise exposure correlates to changes in cortical network connectivity**

Experimental results revealed significant changes in average spontaneous correlation between 13 of a possible 153 cortical ROI combinations after 30 days of CNS that were not observed in control animals. There were further significant changes in eight cortical ROI combinations between the baseline noise and noise after 30 days CNS conditions compared with only three significant changes in controls. These results support the hypothesis that chronic noise exposure can affect cortical networks.

MRI studies of chronically stressed human subjects have documented hyperconnectivity within the default mode network (DMN), which consists of discrete cortical connections between the medial and lateral parietal, mPFC, and medial and lateral temporal cortices that are active during quiet wakefulness (Soares, Sampaio et al. 2013). Psychiatric disorders including PTSD, MDD, and anxiety have been accredited to these stress-induced DMN changes (Golkar, Johansson et al. 2014, Hall, Moda et al. 2015).

Analogous findings have also been reported in MRI studies of spontaneous cortical activity in rodents (Henckens, van der Marel et al. 2015, Grandjean, Azzinnari et al. 2016), and widefield imaging in chronically stressed mice demonstrates that changes in spontaneous cortical glutamate correspond to depressive phenotypes (McGirr, LeDue et al. 2017). Further analysis of network functional connectivity (Jafari, Rezai et al. 2020) with concurrent behavioural measures would be needed to conclude that chronic noise exposure induces behavioural changes related to hyperconnectivity in resting-state networks, but the findings of this thesis are consistent with literature reports and suggest that chronic noise exposure is sufficient to induce breakdown of proper network functioning.

Correlational analysis also revealed significant changes between the spontaneous and noise recording conditions for four cortical ROIs in animals exposed to 30 days CNS. No significant changes were found in control animals or in baseline recordings of either group, indicating that CNS affected the cortical response to acute noise exposure. This finding is consistent with reports that a chronic allostatic load may impair the brain's ability to cope with stress events; a symptom of stress-related disorders including anxiety and depression (McEwen 2004, Dallman and Hellhammer 2010). Acute stress in otherwise healthy subjects induces a transient increase in cortical network activity for enhanced processing of environmental stimuli (Yuen, Liu et al. 2009). Chronic hyperactivity of these networks may increase sensory processing beyond an optimal threshold, altering cortical maps by disrupting neuroplasticity and amplifying sensory noise (Liston, McEwen et al. 2009, Hermans, Henckens et al. 2014). This sensory amplification has also been implicated in the somatosensory symptoms of MDD, related to greater sensory-evoked response variability of cortical networks (McGirr, LeDue et al. 2020).

#### **3.4. Chronic and acute noise exposure alters HPC-BLA connectivity**

When BLA-vHPC theta synchrony was analyzed, a significant shift towards the BLA leading theta activity was found from the baseline spontaneous to the baseline noise conditions in both the control and CNS groups. This shift towards the BLA leading in the presence of an acute stress event (noise exposure during the recording) indicates that BLA-vHPC connectivity is more susceptible to stress-induced alterations than cortical networks. This also supports the hypothesis that noise exposure decreases BLA-vHPC

theta synchrony, where decreased synchrony is defined as a significant deviation from zero leading/lagging time.

There are two types of theta activity. Type 1, or atropine-resistant theta occurs during active periods and is associated with voluntary movement (Kramis, Vanderwolf et al. 1975). Type 2, or atropine-sensitive theta, occurs during periods of behavioural immobility and is associated with freezing and alertness (Karakas 2020). Theta activity during head-fixed movement was filtered from analysis, therefore the theta measures used for analysis were likely type 2.

A shift towards BLA leading theta activity was also found between the spontaneous and noise recording conditions in control animals after 30 days without stress, but not in CNS animals after 30 days of chronic noise exposure. BLA-vHPC synchrony after 30 days CNS shifted significantly closer to zero lead/lag time from the spontaneous to noise recording conditions, but with the BLA still leading. This shift towards BLA leading from baseline spontaneous to spontaneous activity after 30 days CNS indicates that chronic noise exposure was correlated with a change in BLA-vHPC functioning consistent with the response reported for acute stressors. This change in functioning supports the hypothesis that CNS can decrease theta synchrony between the BLA and vHPC, representative of stress-induced alterations of network functioning.

The modulation account of amygdala function postulates that the amygdala is responsible for enhancing emotional memory consolidation by facilitating neural plasticity and information storage (Hermans, Battaglia et al. 2014). The hippocampus and BLA have been shown to activate mechanisms of neuroplasticity during an emotional experience, which are thought to promote the consolidation of long-lasting memories (Diamond,

Campbell et al. 2007, Godoy, Rossignoli et al. 2018). Memory consolidation requires synchronous activity within neuronal ensembles, which facilitates communication between cell populations and mechanisms of synaptic plasticity. A loss of this synchrony towards amygdala hyperactivity may alter the way in which memories are consolidated, resulting in psychological symptoms characteristic of stress-related disorders.

Human neuroimaging studies have shown increased activity in the amygdala immediately following an acute stress event, and also with a pharmacological increase in circulating stress hormones (Hermans, Henckens et al. 2014). Acute immobilization stress in rats has also been shown to decrease coherence between the amygdala and CA1, with the amygdala leading hippocampal theta activity (Hegde, Singh et al. 2008). This increased responsivity is thought to be reflective of the amygdala's function in enhancing emotional memory consolidation, consistent with the BLA leading vHPC activity between the spontaneous and noise recording conditions in both groups. Enhanced explicit and consciously accessible memory can be adaptive in enhancing cognition and determining which emotional stimuli to attend to (Desmedt, Marighetto et al. 2015).

Chronic stress studies have also documented dominance of amygdala activity over hippocampal activity in the absence of an immediate stressor (Ghosh, Laxmi et al. 2013), but this increase in amygdala activity may surpass an optimum threshold. This effect was observed in the shift in the average probability of BLA-vHPC leading/lagging towards the BLA in the spontaneous activity of CNS animals after 30 days noise exposure compared with their baseline recordings. Chronic stress-induced hyperactivity of the amygdala may contribute to ruminative thoughts characteristic of MDD and anxiety, and invasive

emotional memories characteristic of PTSD (Harrington and Blankenship 2006, Bomyea and Lang 2016).

## 4. Conclusion

This thesis examined the effects of chronic noise stress on connectivity within the neocortex, and between the basolateral amygdala and ventral hippocampus. This research was novel in using the same source of chronic stress to activate neural networks during recording to observe the behavioural, cortical, and limbic responses to acute stress exposure. This experimental design has implications not only for stress-related behavioural pathologies including anxiety and depression, but also for PTSD which is characterized by extreme behavioural and psychological reactions to triggers; stimuli reminiscent of the chronic or extreme acute stress event that induced the pathology. Noise is a particularly important research target due to its invasive, inescapable, and growing pervasiveness in modern urban societies (Jariwala, Syed et al. 2017).

Further behavioural, morphological, and network-level stress research could be used to identify the threshold of exposure required to precipitate stress-induced pathologies to inform preventative public health measures, and to identify other factors that could modulate the neural and behavioural chronic stress response. Identifying network-level alterations in brain connectivity also provides a blueprint for targeted and individualized treatments in the future. There is currently no cure for anxiety, depression or PTSD, but chronic stress research informs behavioural, cognitive, and pharmaceutical treatments and preventions for these disorders.

## 5. References

- Afrashteh, N., S. Inayat, E. Bermudez-Contreras, A. Luczak, B. L. McNaughton and M. H. Mohajerani (2020). "Spatiotemporal structure of sensory-evoked and spontaneous activity revealed by mesoscale imaging in anesthetized and awake mice." bioRxiv.
- Alimohammadi, I., F. Ahmadi Kanrash, J. Abolghasemi, H. Afrazandeh and K. Rahmani (2018). "Effect of Chronic Noise Exposure on Aggressive Behavior of Automotive Industry Workers." Int J Occup Environ Med **9**(4): 170-175.
- Antoniuk, S., M. Bijata, E. Ponimaskin and J. Wlodarczyk (2019). "Chronic unpredictable mild stress for modeling depression in rodents: Meta-analysis of model reliability." Neurosci Biobehav Rev **99**: 101-116.
- Basner, M., M. Brink, A. Bristow, Y. de Kluizenaar, L. Finegold, J. Hong, S. A. Janssen, R. Klæboe, T. Leroux, A. Liebl, T. Matsui, D. Schwela, M. Sliwinska-Kowalska and P. Sorqvist (2015). "ICBEN review of research on the biological effects of noise 2011-2014." Noise Health **17**(75): 57-82.
- Belleau, E. L., M. T. Treadway and D. A. Pizzagalli (2019). "The Impact of Stress and Major Depressive Disorder on Hippocampal and Medial Prefrontal Cortex Morphology." Biol Psychiatry **85**(6): 443-453.
- Bermudez-Contreras, E., S. Gomez-Palacio, A. Luczak and M. H. Mohajerani (2020) "Sensory experience selectively reorganizes the late component of evoked responses." DOI: 10.1101/2020.09.30.321547.
- Bomyea, J. and A. J. Lang (2016). "Accounting for intrusive thoughts in PTSD: Contributions of cognitive control and deliberate regulation strategies." J Affect Disord **192**: 184-190.
- Boyle, L. M. (2013). "A neuroplasticity hypothesis of chronic stress in the basolateral amygdala." Yale J Biol Med **86**(2): 117-125.
- Bradley, M. M., Sapigao, R.G., Lang, P.J. (2017). "Sympathetic ANS modulation of pupil diameter in emotional scene perception: Effects of hedonic content, brightness, and contrast." Psychophysiology **54**(10): 1419-1435.
- Britton, J. C., S. Lissek, C. Grillon, M. A. Norcross and D. S. Pine (2011). "Development of anxiety: the role of threat appraisal and fear learning." Depress Anxiety **28**(1): 5-17.
- Brivio, E., J. P. Lopez and A. Chen (2020). "Sex differences: Transcriptional signatures of stress exposure in male and female brains." Genes Brain Behav **19**(3): e12643.
- Brown, E. S., D. J. Woolston and A. B. Froil (2008). "Amygdala volume in patients receiving chronic corticosteroid therapy." Biol Psychiatry **63**(7): 705-709.
- Buzsaki, G. (2002). "Theta oscillations in the hippocampus." Neuron **33**(3): 325-340.
- Buzsaki, G. (2015). "Hippocampal sharp wave-ripple: A cognitive biomarker for episodic memory and planning." Hippocampus **25**(10): 1073-1188.

- Campos, A. C., M. V. Fogaca, D. C. Aguiar and F. S. Guimaraes (2013). "Animal models of anxiety disorders and stress." Braz J Psychiatry **35 Suppl 2**: S101-111.
- Clouter, A., K. L. Shapiro and S. Hanslmayr (2017). "Theta Phase Synchronization Is the Glue that Binds Human Associative Memory." Curr Biol **27**(20): 3143-3148 e3146.
- Dallman, M. F. and D. Hellhammer (2010). Regulation of the hypothalamo-pituitary-adrenal axis, chronic stress, and energy: the role of brain networks. The Handbook of Stress Science: Biology, Psychology, and Health. R. Contrada and A. Baum. New York, NY, Springer: 11-36.
- Desmedt, A., A. Marighetto, G. Richter-Levin and L. Calandreau (2015). "Adaptive emotional memory: the key hippocampal-amygdalar interaction." Stress **18**(3): 297-308.
- Devonshire, I. M., Zheng, Y., Berwick, J. (2014). Voltage-Sensitive Dye Imaging, Intrinsic Optical Signals. Encyclopedia of Computational Neuroscience. J. R. Jaeger D. New York, NY., Springer.
- Diamond, D. M., A. M. Campbell, C. R. Park, J. Halonen and P. R. Zoladz (2007). "The temporal dynamics model of emotional memory processing: a synthesis on the neurobiological basis of stress-induced amnesia, flashbulb and traumatic memories, and the Yerkes-Dodson law." Neural Plast **2007**: 60803.
- Diaz, V. and D. Lin (2020). "Neural circuits for coping with social defeat." Curr Opin Neurobiol **60**: 99-107.
- Dong, Y., Y. Zhou, X. Chu, S. Chen, L. Chen, B. Yang, X. Zhang, L. Wang, S. Wang, J. Lou, Q. Deng, L. Wang, Z. Cao, J. Wang, J. Xie, T. Serdyuk, S. Li, L. He, X. Chen and W. Li (2016). "Dental noise exposed mice display depressive-like phenotypes." Mol Brain **9**(1): 50.
- Dunkley, B. T., S. M. Wong, R. Jetly, J. K. Wong and M. J. Taylor (2018). "Post-traumatic stress disorder and chronic hyperconnectivity in emotional processing." Neuroimage Clin **20**: 197-204.
- Ehlers, J., C. Strauch, J. Georgi and A. Huckauf (2016). "Pupil Size Changes as an Active Information Channel for Biofeedback Applications." Appl Psychophysiol Biofeedback **41**(3): 331-339.
- Ekman, P. (2009). "Darwin's contributions to our understanding of emotional expressions." Philos Trans R Soc Lond B Biol Sci **364**(1535): 3449-3451.
- Feurer, C., K. L. Burkhouse, G. Siegle and B. E. Gibb (2017). "Increased pupil dilation to angry faces predicts interpersonal stress generation in offspring of depressed mothers." J Child Psychol Psychiatry **58**(8): 950-957.
- Fuchs, E., B. Czeh, M. H. Kole, T. Michaelis and P. J. Lucassen (2004). "Alterations of neuroplasticity in depression: the hippocampus and beyond." Eur Neuropsychopharmacol **14 Suppl 5**: S481-490.
- Ghosh, S., T. R. Laxmi and S. Chattarji (2013). "Functional connectivity from the amygdala to the hippocampus grows stronger after stress." J Neurosci **33**(17): 7234-7244.

- Gianaros, P. J., J. R. Jennings, L. K. Sheu, P. J. Greer, L. H. Kuller and K. A. Matthews (2007). "Prospective reports of chronic life stress predict decreased grey matter volume in the hippocampus." Neuroimage **35**(2): 795-803.
- Gilabert-Juan, J., E. Castillo-Gomez, M. Perez-Rando, M. D. Molto and J. Nacher (2011). "Chronic stress induces changes in the structure of interneurons and in the expression of molecules related to neuronal structural plasticity and inhibitory neurotransmission in the amygdala of adult mice." Exp Neurol **232**(1): 33-40.
- Godoy, L. D., M. T. Rossignoli, P. Delfino-Pereira, N. Garcia-Cairasco and E. H. de Lima Umeoka (2018). "A Comprehensive Overview on Stress Neurobiology: Basic Concepts and Clinical Implications." Front Behav Neurosci **12**: 127.
- Godsil, B. P., J. P. Kiss, M. Spedding and T. M. Jay (2013). "The hippocampal-prefrontal pathway: the weak link in psychiatric disorders?" Eur Neuropsychopharmacol **23**(10): 1165-1181.
- Goines, L. and L. Hagler (2007). "Noise pollution: a modern plague." South Med J **100**(3): 287-294.
- Golkar, A., E. Johansson, M. Kasahara, W. Osika, A. Perski and I. Savic (2014). "The influence of work-related chronic stress on the regulation of emotion and on functional connectivity in the brain." PLoS One **9**(9): e104550.
- Grandjean, J., D. Azzinnari, A. Seuwen, H. Sigrist, E. Seifritz, C. R. Pryce and M. Rudin (2016). "Chronic psychosocial stress in mice leads to changes in brain functional connectivity and metabolite levels comparable to human depression." Neuroimage **142**: 544-552.
- Gurumurthy, C. B. and K. C. K. Lloyd (2019). "Generating mouse models for biomedical research: technological advances." Dis Model Mech **12**(1).
- Haines, M. M., S. A. Stansfeld, R. F. Job, B. Berglund and J. Head (2001). "Chronic aircraft noise exposure, stress responses, mental health and cognitive performance in school children." Psychol Med **31**(2): 265-277.
- Hall, B. S., R. N. Moda and C. Liston (2015). "Glucocorticoid Mechanisms of Functional Connectivity Changes in Stress-Related Neuropsychiatric Disorders." Neurobiol Stress **1**: 174-183.
- Hamilton, J. P., M. Siemer and I. H. Gotlib (2008). "Amygdala volume in major depressive disorder: a meta-analysis of magnetic resonance imaging studies." Mol Psychiatry **13**(11): 993-1000.
- Harrington, J. A. and V. Blankenship (2006). "Ruminative thoughts and their relation to depression and anxiety." J. Appl. Soc. Psychol **32**(3): 465-485.
- Hegde, P., K. Singh, S. Chaplot, B. S. Shankaranarayana Rao, S. Chattarji, B. M. Kutty and T. R. Laxmi (2008). "Stress-induced changes in sleep and associated neuronal activity in rat hippocampus and amygdala." Neuroscience **153**(1): 20-30.

- Henckens, M. J., K. van der Marel, A. van der Toorn, A. G. Pillai, G. Fernandez, R. M. Dijkhuizen and M. Joels (2015). "Stress-induced alterations in large-scale functional networks of the rodent brain." Neuroimage **105**: 312-322.
- Henderson, R. R., M. M. Bradley and P. J. Lang (2018). "Emotional imagery and pupil diameter." Psychophysiology **55**(6): e13050.
- Herman, J. P., J. M. McKlveen, S. Ghosal, B. Kopp, A. Wulsin, R. Makinson, J. Scheimann and B. Myers (2016). "Regulation of the Hypothalamic-Pituitary-Adrenocortical Stress Response." Compr Physiol **6**(2): 603-621.
- Herman, J. P., J. G. Tasker, D. R. Ziegler and W. E. Cullinan (2002). "Local circuit regulation of paraventricular nucleus stress integration: glutamate-GABA connections." Pharmacol Biochem Behav **71**(3): 457-468.
- Hermans, E. J., F. P. Battaglia, P. Atsak, L. D. de Voogd, G. Fernandez and B. Roozendaal (2014). "How the amygdala affects emotional memory by altering brain network properties." Neurobiol Learn Mem **112**: 2-16.
- Hermans, E. J., M. J. Henckens, M. Joels and G. Fernandez (2014). "Dynamic adaptation of large-scale brain networks in response to acute stressors." Trends Neurosci **37**(6): 304-314.
- Hoffman, A. N., A. Parga, P. R. Paode, L. R. Watterson, E. M. Nikulina, R. P. Hammer, Jr. and C. D. Conrad (2015). "Chronic stress enhanced fear memories are associated with increased amygdala zif268 mRNA expression and are resistant to reconsolidation." Neurobiol Learn Mem **120**: 61-68.
- Hultman, R., K. Ulrich, B. D. Sachs, C. Blount, D. E. Carlson, N. Ndubuizu, R. C. Bagot, E. M. Parise, M. T. Vu, N. M. Gallagher, J. Wang, A. J. Silva, K. Deisseroth, S. D. Mague, M. G. Caron, E. J. Nestler, L. Carin and K. Dzirasa (2018). "Brain-wide Electrical Spatiotemporal Dynamics Encode Depression Vulnerability." Cell **173**(1): 166-180 e114.
- Jacinto, L. R., J. S. Reis, N. S. Dias, J. J. Cerqueira, J. H. Correia and N. Sousa (2013). "Stress affects theta activity in limbic networks and impairs novelty-induced exploration and familiarization." Front Behav Neurosci **7**: 127.
- Jafari, Z., B. E. Kolb and M. H. Mohajeri (2017). "Effect of acute stress on auditory processing: a systematic review of human studies." Rev Neurosci **28**(1): 1-13.
- Jafari, Z., B. E. Kolb and M. H. Mohajeri (2018). "Chronic traffic noise stress accelerates brain impairment and cognitive decline in mice." Exp Neurol **308**: 1-12.
- Jafari, Z., B. E. Kolb and M. H. Mohajeri (2020). "Noise exposure accelerates the risk of cognitive impairment and Alzheimer's disease: Adulthood, gestational, and prenatal mechanistic evidence from animal studies." Neurosci Biobehav Rev **117**: 110-128.
- Jafari, Z., J. Rezai, N. Afrashteh, R. Torabi, S. Singh, B. E. Kolb, J. Davidsen and M. H. Mohajeri (2020). "Prenatal stress dysregulates resting-state functional connectivity and sensory motifs." bioRxiv.

- Jariwala, H. J., H. S. Syed, M. J. Pandya and Y. M. Gajera (2017). Noise Pollution & Human Health: A Review. Noise and Air Pollution: Challenges and Opportunities.
- Jawabri, K. H. and S. Sharma (2020). Physiology, Cerebral Cortex Functions. StatPearls. Treasure Island (FL).
- Jiang, H., S. Liu, X. Geng, A. Caccavano, K. Conant, S. Vicini and J. Wu (2018). "Pacing Hippocampal Sharp-Wave Ripples With Weak Electric Stimulation." Front Neurosci **12**: 164.
- Joo, H. R. and L. M. Frank (2018). "The hippocampal sharp wave-ripple in memory retrieval for immediate use and consolidation." Nat Rev Neurosci **19**(12): 744-757.
- Kaada, B. R. (1972). Stimulation and Regional Ablation of the Amygdaloid Complex with Reference to Functional Representations. The Neurobiology of the Amygdala. Boston, MA, Springer. **2**: 205-281.
- Kaiser, R. H., J. R. Andrews-Hanna, T. D. Wager and D. A. Pizzagalli (2015). "Large-Scale Network Dysfunction in Major Depressive Disorder: A Meta-analysis of Resting-State Functional Connectivity." JAMA Psychiatry **72**(6): 603-611.
- Karakas, S. (2020). "A review of theta oscillation and its functional correlates." Int J Psychophysiol **157**: 82-99.
- Karimi Abadchi, J., M. Nazari-Ahangarkolae, S. Gattas, E. Bermudez-Contreras, A. Luczak, B. L. McNaughton and M. H. Mohajerani (2020). "Spatiotemporal patterns of neocortical activity around hippocampal sharp-wave ripples." Elife **9**.
- Korn, C. W., M. Staib, A. Tzovara, G. Castegnetti and D. R. Bach (2017). "A pupil size response model to assess fear learning." Psychophysiology **54**(3): 330-343.
- Kramis, R., C. H. Vanderwolf and B. H. Bland (1975). "Two types of hippocampal rhythmical slow activity in both the rabbit and the rat: relations to behavior and effects of atropine, diethyl ether, urethane, and pentobarbital." Exp Neurol **49**(1 Pt 1): 58-85.
- Lamb, D. H. (1979). "On the Distinction Between Physical and Psychological Stressors." Motivation and Emotion **3**(1): 51-61.
- Lange, C. and E. Irlé (2004). "Enlarged amygdala volume and reduced hippocampal volume in young women with major depression." Psychol Med **34**(6): 1059-1064.
- Lee, C. R. and D. J. Margolis (2016). "Pupil Dynamics Reflect Behavioral Choice and Learning in a Go/NoGo Tactile Decision-Making Task in Mice." Front Behav Neurosci **10**: 200.
- Lee, T., T. Jarome, S. J. Li, J. J. Kim and F. J. Helmstetter (2009). "Chronic stress selectively reduces hippocampal volume in rats: a longitudinal magnetic resonance imaging study." Neuroreport **20**(17): 1554-1558.
- Leuchs, L., M. Schneider, M. Czisch and V. I. Spormaker (2017). "Neural correlates of pupil dilation during human fear learning." Neuroimage **147**: 186-197.

- Li, Y., J. Qin, J. Yan, N. Zhang, Y. Xu, Y. Zhu, L. Sheng, X. Zhu and S. Ju (2019). "Differences of physical vs. psychological stress: evidences from glucocorticoid receptor expression, hippocampal subfields injury, and behavioral abnormalities." Brain Imaging Behav **13**(6): 1780-1788.
- Lin, Y., G. J. Ter Horst, R. Wichmann, P. Bakker, A. Liu, X. Li and C. Westenbroek (2009). "Sex differences in the effects of acute and chronic stress and recovery after long-term stress on stress-related brain regions of rats." Cereb Cortex **19**(9): 1978-1989.
- Liston, C., B. S. McEwen and B. J. Casey (2009). "Psychosocial stress reversibly disrupts prefrontal processing and attentional control." Proc Natl Acad Sci U S A **106**(3): 912-917.
- Liu, W. Z., W. H. Zhang, Z. H. Zheng, J. X. Zou, X. X. Liu, S. H. Huang, W. J. You, Y. He, J. Y. Zhang, X. D. Wang and B. X. Pan (2020). "Identification of a prefrontal cortex-to-amygdala pathway for chronic stress-induced anxiety." Nat Commun **11**(1): 2221.
- Malone, B. J., M. A. Heiser, R. E. Beitel and C. E. Schreiner (2017). "Background noise exerts diverse effects on the cortical encoding of foreground sounds." J Neurophysiol **118**(2): 1034-1054.
- Maren, S. and A. Holmes (2016). "Stress and Fear Extinction." Neuropsychopharmacology **41**(1): 58-79.
- Marvin, J. S., B. G. Borghuis, L. Tian, J. Cichon, M. T. Harnett, J. Akerboom, A. Gordus, S. L. Renninger, T. W. Chen, C. I. Bargmann, M. B. Orger, E. R. Schreiter, J. B. Demb, W. B. Gan, S. A. Hires and L. L. Looger (2013). "An optimized fluorescent probe for visualizing glutamate neurotransmission." Nat Methods **10**(2): 162-170.
- McDonald, A. J. (1998). "Cortical pathways to the mammalian amygdala." Prog Neurobiol **55**(3): 257-332.
- McEwen, B. S. (2004). "Protection and damage from acute and chronic stress: allostasis and allostatic overload and relevance to the pathophysiology of psychiatric disorders." Ann N Y Acad Sci **1032**: 1-7.
- McEwen, B. S. (2006). "Protective and damaging effects of stress mediators: central role of the brain." Dialogues Clin Neurosci **8**(4): 367-381.
- McEwen, B. S. (2007). "Physiology and neurobiology of stress and adaptation: central role of the brain." Physiol Rev **87**(3): 873-904.
- McEwen, B. S. (2017). "Neurobiological and Systemic Effects of Chronic Stress." Chronic Stress (Thousand Oaks) **1**.
- McGirr, A., J. LeDue, A. W. Chan, J. D. Boyd, P. D. Metzack and T. H. Murphy (2020). "Stress impacts sensory variability through cortical sensory activity motifs." Transl Psychiatry **10**(1): 20.
- McGirr, A., J. LeDue, A. W. Chan, Y. Xie and T. H. Murphy (2017). "Cortical functional hyperconnectivity in a mouse model of depression and selective network effects of ketamine." Brain **140**(8): 2210-2225.

- McLaughlin, K. J., S. E. Baran and C. D. Conrad (2009). "Chronic stress- and sex-specific neuromorphological and functional changes in limbic structures." Mol Neurobiol **40**(2): 166-182.
- Menon, V. (2011). "Large-scale brain networks and psychopathology: a unifying triple network model." Trends Cogn Sci **15**(10): 483-506.
- Mohajerani, M. H., A. W. Chan, M. Mohsenvand, J. LeDue, R. Liu, D. A. McVea, J. D. Boyd, Y. T. Wang, M. Reimers and T. H. Murphy (2013). "Spontaneous cortical activity alternates between motifs defined by regional axonal projections." Nat Neurosci **16**(10): 1426-1435.
- Montgomery, S. M., M. I. Betancur and G. Buzsaki (2009). "Behavior-dependent coordination of multiple theta dipoles in the hippocampus." J Neurosci **29**(5): 1381-1394.
- Moustafa, A. A., M. W. Gilbertson, S. P. Orr, M. M. Herzallah, R. J. Servatius and C. E. Myers (2013). "A model of amygdala-hippocampal-prefrontal interaction in fear conditioning and extinction in animals." Brain Cogn **81**(1): 29-43.
- Munzel, T., A. Daiber, S. Steven, L. P. Tran, E. Ullmann, S. Kossmann, F. P. Schmidt, M. Oelze, N. Xia, H. Li, A. Pinto, P. Wild, K. Pies, E. R. Schmidt, S. Rapp and S. Kroller-Schon (2017). "Effects of noise on vascular function, oxidative stress, and inflammation: mechanistic insight from studies in mice." Eur Heart J **38**(37): 2838-2849.
- Naqvi, F., S. Haider, Z. Batool, T. Perveen and D. J. Haleem (2012). "Sub-chronic exposure to noise affects locomotor activity and produces anxiogenic and depressive like behavior in rats." Pharmacol Rep **64**(1): 64-69.
- Nollet, M., A. M. Le Guisquet and C. Belzung (2013). "Models of depression: unpredictable chronic mild stress in mice." Curr Protoc Pharmacol **Chapter 5**: Unit 5 65.
- Orem, T. R., M. D. Wheelock, A. M. Goodman, N. G. Harnett, K. H. Wood, E. W. Gossett, D. A. Granger, S. Mrug and D. C. Knight (2019). "Amygdala and prefrontal cortex activity varies with individual differences in the emotional response to psychosocial stress." Behav Neurosci **133**(2): 203-211.
- Patel, D., M. J. Kas, S. Chattarji and B. Buwalda (2019). "Rodent models of social stress and neuronal plasticity: Relevance to depressive-like disorders." Behav Brain Res **369**: 111900.
- Pawlak, R., B. S. Rao, J. P. Melchor, S. Chattarji, B. McEwen and S. Strickland (2005). "Tissue plasminogen activator and plasminogen mediate stress-induced decline of neuronal and cognitive functions in the mouse hippocampus." Proc Natl Acad Sci U S A **102**(50): 18201-18206.
- Paxinos, G. and K. B. J. Franklin (2001). The Mouse Brain in Stereotaxic Coordinates, Academic Press.
- Pittenger, C. and R. S. Duman (2008). "Stress, depression, and neuroplasticity: a convergence of mechanisms." Neuropsychopharmacology **33**(1): 88-109.

- Reimer, J., M. J. McGinley, Y. Liu, C. Rodenkirch, Q. Wang, D. A. McCormick and A. S. Tolia (2016). "Pupil fluctuations track rapid changes in adrenergic and cholinergic activity in cortex." Nat Commun **7**: 13289.
- Riga, D., M. R. Matos, A. Glas, A. B. Smit, S. Spijker and M. C. Van den Oever (2014). "Optogenetic dissection of medial prefrontal cortex circuitry." Front Syst Neurosci **8**: 230.
- Rosenkranz, J. A., E. R. Venheim and M. Padival (2010). "Chronic stress causes amygdala hyperexcitability in rodents." Biol Psychiatry **67**(12): 1128-1136.
- Rosenthal, N. and S. Brown (2007). "The mouse ascending: perspectives for human-disease models." Nat Cell Biol **9**(9): 993-999.
- Schriver, B. J., S. Bagdasarov and Q. Wang (2018). "Pupil-linked arousal modulates behavior in rats performing a whisker deflection direction discrimination task." J Neurophysiol **120**(4): 1655-1670.
- Seidler, A., J. Hegewald, A. L. Seidler, M. Schubert, M. Wagner, P. Droge, E. Haufe, J. Schmitt, E. Swart and H. Zeeb (2017). "Association between aircraft, road and railway traffic noise and depression in a large case-control study based on secondary data." Environ Res **152**: 263-271.
- Selye, H. (1950). "Stress and the general adaptation syndrome." Br Med J **1**(4667): 1383-1392.
- Sharp, B. M. (2017). "Basolateral amygdala and stress-induced hyperexcitability affect motivated behaviors and addiction." Transl Psychiatry **7**(8): e1194.
- Sheline, Y. I., C. Liston and B. S. McEwen (2019). "Parsing the Hippocampus in Depression: Chronic Stress, Hippocampal Volume, and Major Depressive Disorder." Biol Psychiatry **85**(6): 436-438.
- Simmons, D. (2008). "The use of animal models in studying genetic disease: transgenesis and induced mutation." Nature Education **1**(1): 70.
- Singh, S., E. Bermudez-Contreras, M. Nazari, R. J. Sutherland and M. H. Mohajerani (2019). "Low-cost solution for rodent home-cage behaviour monitoring." PLoS One **14**(8): e0220751.
- Soares, J. M., A. Sampaio, L. M. Ferreira, N. C. Santos, P. Marques, F. Marques, J. A. Palha, J. J. Cerqueira and N. Sousa (2013). "Stress Impact on Resting State Brain Networks." PLoS One **8**(6): e66500.
- Soltani Zangbar, H., T. Ghadiri, M. Seyedi Vafae, A. Ebrahimi Kalan, S. Fallahi, M. Ghorbani and P. Shahabi (2020). "Theta Oscillations Through Hippocampal/Prefrontal Pathway: Importance in Cognitive Performances." Brain Connect **10**(4): 157-169.
- Stallen, P. J. (1999). "A theoretical framework for environmental noise annoyance." Noise Health **1**(3): 69-80.

- Stein, J. L., L. M. Wiedholz, D. S. Bassett, D. R. Weinberger, C. F. Zink, V. S. Mattay and A. Meyer-Lindenberg (2007). "A validated network of effective amygdala connectivity." Neuroimage **36**(3): 736-745.
- Stujenske, J. M., E. Likhtik, M. A. Topiwala and J. A. Gordon (2014). "Fear and safety engage competing patterns of theta-gamma coupling in the basolateral amygdala." Neuron **83**(4): 919-933.
- Supcun, B., M. K. Ghadiri, M. Zeraati, W. Stummer, E. J. Speckmann and A. Gorji (2012). "The effects of tetanic stimulation on plasticity of remote synapses in the hippocampus-perirhinal cortex-amygdala network." Synapse **66**(11): 965-974.
- Takagi, Y., Y. Sakai, Y. Abe, S. Nishida, B. J. Harrison, I. Martinez-Zalacain, C. Soriano-Mas, J. Narumoto and S. C. Tanaka (2018). "A common brain network among state, trait, and pathological anxiety from whole-brain functional connectivity." Neuroimage **172**: 506-516.
- Tian, L., S. A. Hires, T. Mao, D. Huber, M. E. Chiappe, S. H. Chalasani, L. Petreanu, J. Akerboom, S. A. McKinney, E. R. Schreiter, C. I. Bargmann, V. Jayaraman, K. Svoboda and L. L. Looger (2009). "Imaging neural activity in worms, flies and mice with improved GCaMP calcium indicators." Nat Methods **6**(12): 875-881.
- Westman, J. C. and J. R. Walters (1981). "Noise and stress: a comprehensive approach." Environ Health Perspect **41**: 291-309.
- Winson, J. and C. Abzug (1978). "Neuronal transmission through hippocampal pathways dependent on behavior." J Neurophysiol **41**(3): 716-732.
- Witter, M. (2012). Hippocampus. The Mouse Nervous System. P. G. Watson C., Puelles, L, Academic Press: 112-139.
- Xie, Y., A. W. Chan, A. McGirr, S. Xue, D. Xiao, H. Zeng and T. H. Murphy (2016). "Resolution of High-Frequency Mesoscale Intracortical Maps Using the Genetically Encoded Glutamate Sensor iGluSnFR." J Neurosci **36**(4): 1261-1272.
- Yamanaka, K. and M. Kawakami (2009). "Convenient evaluation of mental stress with pupil diameter." Int J Occup Saf Ergon **15**(4): 447-450.
- Yang, Y. and J. Z. Wang (2017). "From Structure to Behavior in Basolateral Amygdala-Hippocampus Circuits." Front Neural Circuits **11**: 86.
- Young, A. H. (2004). "Cortisol in mood disorders." Stress **7**(4): 205-208.
- Yuen, E. Y., W. Liu, I. N. Karatsoreos, J. Feng, B. S. McEwen and Z. Yan (2009). "Acute stress enhances glutamatergic transmission in prefrontal cortex and facilitates working memory." Proc Natl Acad Sci U S A **106**(33): 14075-14079.
- Zhang, X., T. T. Ge, G. Yin, R. Cui, G. Zhao and W. Yang (2018). "Stress-Induced Functional Alterations in Amygdala: Implications for Neuropsychiatric Diseases." Front Neurosci **12**: 367.